International Journal of Science and Engineering Applications
Volume 7–Issue 06, 71-79, 2018, ISSN:-2319–7560

Optimal Location of Distributed Generation Sources and Capacitance of Distribution Network to Reduce Losses, Improve Voltage Profile, and Minimizing the Costs Using Genetic and Harmonic Search Algorithm

Mahdi Mansouri
MSc of Executive Management, Marketing Strategy, Islamic Azad University
Ahar, East Azarbaijan, Iran

Hosein Gholizadeh
Dept. of Electrical Engineering, Islamic Azad University Central Tehran Branch College
Tehran, Iran

Abstract: Reducing losses and improving the voltage profile have been the main objectives of electrical power system designers. One of the suggested solutions for achieving these goals is the use of parallel capacitors and distributed generation sources in distribution systems. A location that is optimized for DG installation may not be the best place to minimize losses in improving the system voltage profile. In this paper, determining the optimal location of the dispersed generation unit and the capacitive bank with the goal of optimizing a target function, including losses, improving the voltage profile, and the cost of investment in capacitors and dispersed production. In this paper, IEEE standard 33 buses is considered for simulation, and the results are obtained by using genetic and harmonic search algorithm indicate that DG optimization and capacitor with a target function in which the loss reduction and improvement of the voltage profile is considered to reduce costs, reduce losses, and improve the voltage profile, which are remarkable improvements.

Keywords: Optimal Placement; Distributed Generation; Genetic Algorithm; Voltage Profile; Harmonic Search Algorithm;

1. INTRODUCTION

Renewable energies are becoming more common as because of increasing electricity demand. Optimal placement of Distributed generation (DG) in power systems has high importance for improving voltage stability, reducing loses, and minimizing the costs [1].

Reducing losses and improving the voltage profile is one of the most important issues in the power industry. There is also a large share of energy losses in the distribution sector, which is equivalent to about 75% of the data in this area. Therefore, consideration of issues such as location, capacitance, and re-networking are essential. Distributed generation generally refers to low power generation sources, typically between KW1 to MW50 that are located near the consumer location or connected to the distribution network [2-4]. One of the important issues in distributed generation studies is the problem of placement and determination of their capacity. The disposition of the dispersed production on the power transmission and the number of losses is significant [5, 6]. Due to the network's electrical parameters, load distribution equations, and the constraints on the use of distributed generation sources, the problem of displacement will have some characteristics that, from an optimization perspective, are some of these characteristics:

- The resulting equations are nonlinear [7].
- The variable of a state that can predict the existence or absence of a source is a discrete variable. The variable of a state that can predict the existence or absence of a Distributed generation source in a bus-bar is a discrete variable [8].
- Since there is virtually no capacity for installation, and the source cannot be dispersed in each shin, the target function is a discontinuous function [9].
- For real networks, the problem becomes an issue for a very large dimensional problem [10].

Capacitors are used as one of the most economical methods for increasing the electrical power quality so that the optimal location of this element has a significant effect on the transmission power, the loss of lines, the voltage profile, and the reliability of the network [11-14]. Static voltage stability of grid in south-east Iran power system has been conducted in [15-17]. Extended continuation power flow is used to get more accurate results in this system.

The use of parallel capacitors and distributed generation in the distribution system to increase the electrical power quality and reduce the cost of the system in the system has always been one of the important issues for engineers [18]. The installation of parallel capacitors and distributed generation generators will have many benefits for manufacturers and consumers of electrical energy, which will be referred to later in this chapter. Maximum access to the above benefits depends on how they are installed in the distribution system since their optimal placement has a great influence on the power transmission, the number of line losses, the voltage profile, and the reliability of the network. On the other hand, improper placement of distributed generation generators in the system will cause disadvantages such as increasing losses, reducing voltage and increasing costs [19].

Therefore, the problem of determining the location and optimal capacity size of capacitor banks and distributed generation should be addressed, which is referred to as the

problem of optimal placement of capacitors and distributed generation. Hence, various methods have been proposed by researchers in different scientific institutions for the last decades [20]. In this chapter, first, a brief summary of capacitors and distributed generation are described. Then, a brief overview of the above methods and the work done so far is discussed.

As you can see, two of the objective profit target functions and the voltage profile indicator for this issue are considered. In most articles, a function is called the cost function using the following formula.

$$F = \sum_{i=1}^{nb} k_p \cdot P_{loss}^{i} + \sum_{j=1}^{nc} k_c \cdot Q_c^{j} \quad (1)$$

In which, P_{loss}^{i} is loss in section i, nb is the numbers of sections in the network, Q_c^{j} is the value for capacitance in section j, nc is the numbers of capacitors, k_p is the expense of power per kW, and k_c is the cost of capacitor per KVAR. Casualties in the distribution network include two parts of power and energy. The power losses are related to peak loading and the energy losses associated with loading over a period (one year), which can be calculated using the loss factor of peak losses. Kp is the total cost of power and energy losses per kw of peak losses. After the capacitance, the gain from the capacitance in the network can also be calculated by using the following formula, which is presented as the main objective function in the capacitance.

$$S = k_e \times 8760 \times LSF\left(P_l - P_l^{c}\right) - \sum_{i=1}^{nc} k_c . Q_{ci} \quad (2)$$

In which, k_e is the cost of energy losses, LSF is loss factor, P_l is courier loss before capacitance, P_l^{c} is Peak losses are after capacitance. Table 3 also shows information about this objective function, as well as the profit function. The exploitation of distribution networks in normal conditions due to appropriate protection coordination, limiting the network interface level and the problems of exploiting interconnected networks, are often carried out radially, and the numerous disconnect switches available on the network play a significant role in Network structure management functions to achieve optimal form. Replacing or changing the arrangement in the distribution network, changing the arrangement of feeders, opening and closing switches (power switches, removable and non-removable actuators under load, etc.) to change the topology of the network.

2. OBJECTIVE FUNCTION

2.1 Loss

The casualty has various causes, part of which is the main part of it, is part of the essence of the network. Because everywhere there is a network of conductors, casualties are inevitable due to the flow of conductors. The first objective function is the active loss of the feeders of the distribution network, which is expressed as:

$$\min P_{loss} = \sum_{i=1}^{n_p} r_i \frac{P_i^2 + Q_i^2}{V_i^2} \quad (3)$$

In which, n_p is a total number of network branches, r_i is the resistance of branch I, Q_i is the reactive power of branch i, P_i is the active power of branch I, and V_i is the voltage of branch i.

2.2 Voltage

From the perspective of consumers, having a voltage in the limit is one of the important factors in the quality of electricity. Radial networks at the end of their own usually suffer from a weak voltage. Replacing with the change in the flow path, it can modify the voltage profile to a certain extent, which is almost synonymous with loss reduction [21]. The next target function is related to the voltage profile indicator, the mathematical formulation of which is expressed as follows:

$$\min V_s = \sqrt{\frac{1}{n} \sum_{i=1}^{n_b} (V_i - V_p)^2} \quad (4)$$

$$V_p = \frac{1}{n} \times \sum_{i=1}^{n_b} V_i \quad (5)$$

In which, V_s is voltage index, V_i, the voltage of branch i, n_b is the number of network nodes, and V_p is Average node voltage.

3. CONSTRAINTS

In all optimization steps, the following constraints should be considered [22-24]:

1. The radial constraint of the grid: In all the matching arrangements, the grid must always maintain its radial structure.
2. Node Voltage Limit Constraint: $V_{i\,\min} \le V_i \le V_{i\,\max}$
3. Limitation of the flow of branches: $I_n \langle I_{n\,\max}$
4. All nodes are always energized: All network nodes in the arrays obtained from the algorithm should always be light and not isolated in the network.

4. OPTIMIZATION METHODS

4.1 Genetic Algorithm

Genetic algorithms are based on chromosomes and their natural evolution. In this method, contrary to the analytical methods, try and error, instead of working on an optimal answer, they work on several answers that they call "populations". As a result, the problem space is searched more effectively. Also, search and evolutionary operations take place on the coded state of the answers, which is generally binary coding. A specific feature of the way genetic algorithms is based on solving optimization problems is that these methods have high efficiency in the absence of specific information about the problem or the need for specific conditions of the response space such as uniformity, convexity, and single-valuedness [25, 26].

Another important feature of these algorithms in terms of computational programming is that each member of the population does not respond to other members and

independently evolves. Therefore, in solving complex and heavy problems, parallel processors and the robust controller can be used to quickly solve the problem [27].

In the case of the economic distribution of the load, given that we have N units of production, we consider N-1 unit (variable) because, with the capability of producing N-1 units, the production capacity of unit N, which is also Pref We can call it the form (6). Generally, Pref is divided into units whose production range (ie, Pmin-Pmax) is higher than other units.

$$P_{ref} = P_L - \sum_{i=1}^{N-1} P_1 \quad (6)$$

In this paper, binary coding is used to apply the genetic algorithm to solve the problem of economic distribution of charge, and each chromosome, resulting from the combining of the encoded string of numerical values of N-1 varies. In the above problem, the length of the encoded string of the variable i is the smallest integer corresponding to (7).

$$2^{m-1} \langle \left(P_{i,\max} - P_{i,\min} \right) \times 10^i \le 2^m - 1 \quad (7)$$

In which, m_i is The length of the i-th encoded variable, $P_{i,max}$ is produced power, $P_{i,min}$ is the minimum produced power, and I is the number of digits after decimals. After joining the encoded fields of variables, the chromosome contains the coded values of all the variables. Therefore, the length of the chromosomes of the algorithm can be determined from equation (8).

$$L = \sum_{i-1}^{N-1} m_i \quad (8)$$

Obviously, with the increase in the number of chromosome production units of the algorithm, the amount of memory in the system increases linearly. Also, to return the chromosome to true values of the problem variables, first each chromosome is divided into the corresponding coding sequences, and then we use equation (9).

$$P_1 = P_{i,\min} + \text{decimal (substring)} \times \frac{P_{i,\max} - p_{i,\min}}{2^m - 1} \quad (9)$$

The initial population of the genetic algorithm is randomly formed, and then the following evolutionary processes occur on a population and a new generation emerges:

- Roulette cycle: In this process, population chromosomes are selected with a probability proportional to the chromosomal fitness (value of the target function) [28]. In this process, chromosomes may be selected more than once (a strong chromosome) or chromosomes never to be selected (weak chromosome) [29].
- Cross-over: In this process, two parent chromosomes are produced by two child chromosomes [30]. The simplest algorithm for this process is the discontinuous cutting algorithm. This process takes place with the probability of a p_c population [31].
- Mutation: During this process, several genes (bits) of chromosomes of the population change from one to zero, or vice versa, from zero to one [32]. This process is applied to the population with a small probability of p_m [33].

In the first process, chromosomes of the population converge to the superior chromosomes (or chromosomes). In the second process, the child's chromosomes create the properties of their parents and direct the algorithm to the optimum point. To move faster towards the optimal point, it's best to always have one parent, the best chromosome of the generation. In the third process, it is possible to enter chromosomes whose probability of entry into the algorithm is very low and may even be the optimal solution to the problem. The probability of this process should be low so that the algorithm does not find a random process. As it is obvious, the coupling process causes the convergence and the mutation process causes the divergence of the algorithm. Therefore, for the fastest convergence, one can estimate the overall fitness of a generation in each generation and correct the probabilities of Pc and Pm for future generations. An important point to note is that there may be a chromosomal algorithm that does not belong to the response space. In such a case, in the case of the economic distribution of time, there is no time for which Pref does not fall within its scope of production, namely:

$$P_{ref} \notin \left| P_{\min,ref}, P_{\max,ref} \right| \quad (10)$$

In this case, we must remove the chromosome and replace the other chromosome. This process is corrected as linear. The genetic algorithm cycle is presented in the flowchart of figure 1.

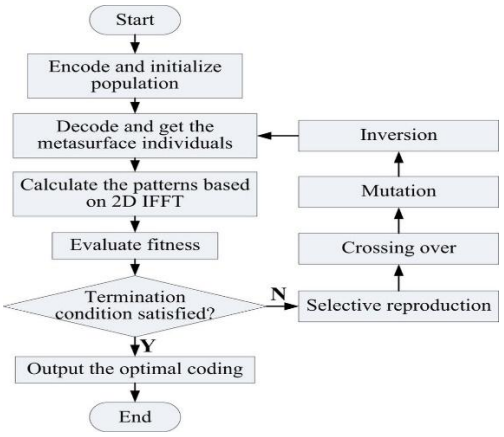

Figure 1. Genetic Algorithm flowchart

4.2 Harmonic Search Algorithm

Nowadays, with increasing issues and the importance of speeding up the response and failure to respond to classical methods, the search algorithms of the full-scale problem space are welcome. In the meantime, the use of hyper surfing (intuitive) search algorithms also has an inherited growth algorithm, ants colony algorithm, and so on [34]. Due to the unique features of the Harmonic Search Algorithm (HSA), this search method has been used.

Characteristics of the Harmony Search Algorithm are:

- There is no need to search for the initial value, and the problem is not trapped in the optimal local response [35].
- Instead of searching for a derivative of random search, an optimal answer is used [36].
- In contrast to derivative-based optimization methods, in addition to continuous variables, it has the ability to work with discrete variables [37].

- Also, the Harmonic Search algorithm uses some of the features of other meta-innovative algorithms, such as preserving previous vectors of a similar taboo search algorithm (TS), providing harmonic memory from the start to the end of simulated cooking (SA) and evaluating multiple Vector at the same time as the inheritance algorithm. But compared to them, they have less mathematical prerequisites and the ability to solve various engineering optimizations. The Harmonic Search algorithm creates a new answer after considering all the answers. While the inheritance algorithm considers only two parent polynomials, this flexibility increases the search algorithm's harmony and results in the optimal answer.

The steps in which the algorithm searches for harmonics for optimization is that in the first step, initialization of the problem parameters and algorithm is performed; in the second and third steps, the initialization of the first harmonic memory (HM) and the creation of a new harmony respectively Harmony memory is performed; in the next steps, updating the harmonic memory and checking the stop condition is done. The parameters of the Harmony Search Algorithm, which can have different values in each issue. The intended settings for the Harmony Search Algorithm include the size of the Harmonic Memory (HMS), the speed of the Harmonic Memory Check (HMCR), the Bandwidth Parameter Parameterization (Bw), the Manufacturing Numbers (NI) in Table 2 [38-44].

Table 1. Harmonic search algorithm parameters

Parameter	
HMS	10
HMCR	0/85
PAR	0/3

The flowchart and algorithm process are shown in Figure 2.

5. SYSTEM'S MODEL

In this paper, six scenarios for solving the problem of repositioning and capacitance (four capacitors with a capacity of 50kvar) and distributed generation sources have been investigated to reduce losses and improve the voltage profile of an IEEE 33base network. Information about the distributed source is shown with the specifications specified in Table (2). Specifications for the objective function. The cost of loss and profit from the condensation are shown in Table (3).

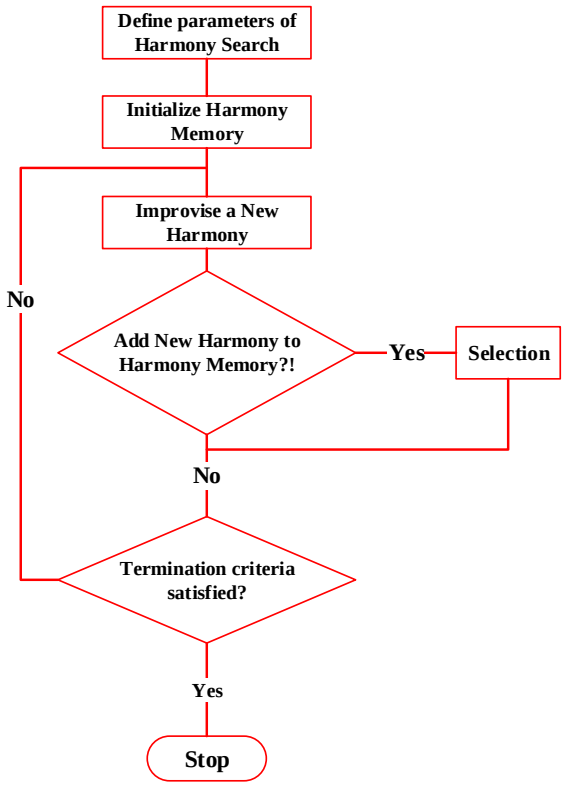

Figure 2. The flowchart of Harmonic Search Algorithm

Table 2. The initial location of the distributed production resources and their size

33-Bus Installation node and capacity of DG	
Node	Capacity(kw/p.f)
3	50/0.8
6	100/0.9
24	200/0.9
29	100/1

Table 3. Information about the objective function of the cost of loss and profit

Parameter	Value
k_p ($/kw)	120
k_c ($/kvar)	5
k_e ($/kwh)	0.3
LSF	0.554

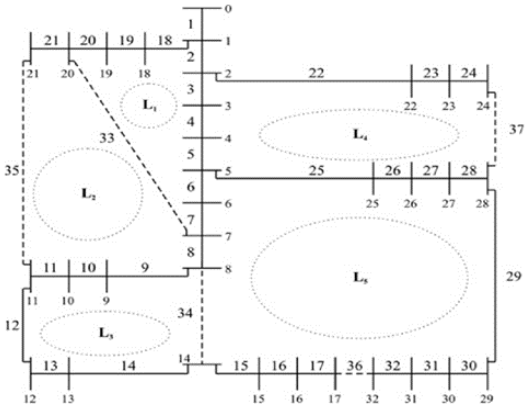

Figure 3. IEEE 33-buses system

6. SIMULATION RESULTS

In the first scenario, the network openness was researched with the assumption that the location of distributed sources of production was constant (Table 2), the active network losses in the presence and absence of distributed generation sources.

Table 4. The 33-bus network active casualties without the presence of distributed generation sources

	open switch	Ploss (KW)	Reduction (%)
initial	s33,s34,s35,s36,s37	202.5	-
GA	s7,s9,s14,s32,s37	139.5	31.11
HS	s7,s9,s14,s28,s32	139.9	30.91

Table 5. The 33-bus network active casualties in the presence of distributed generation sources

	open switch	Ploss (KW)	Reduction (%)
initial	s33,s34,s35,s36,s37	169.75	-
GA	s7,s9,s14,s28,s32	115.72	31.82
HS	s7,s10,s14,s28,s32	116.44	31.41

The presence of these resources in the same initial arrangement has reduced losses from 202.5 kV to 169.75 kW. But after applying the rearrangement in both of these ways, losses from the original arrangement were significantly reduced by two algorithms. Network losses have been reduced by 31.82 percent using a genetic algorithm and also with Harmonic Search Algorithm, with a very near-optimal reduction of 31.41 percent. In the case comparison case, the casualties achieved for the optimal arrangement of genetic algorithms in the absence of distributed sources of resources have reached 139.5 to 115.72 in the presence of these resources. And the impact of the presence of these resources is quite visible.

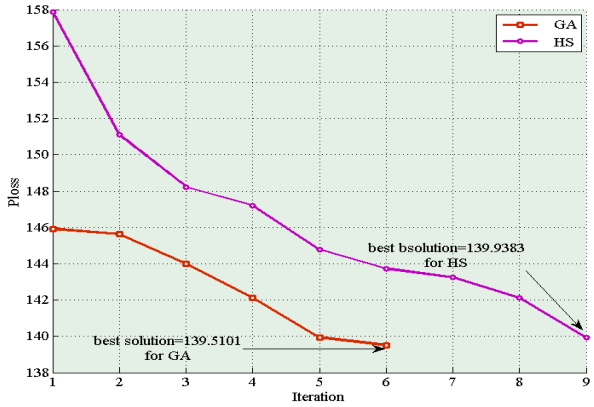

Figure 4. Comparison of the convergence diagrams of 2 algorithms for the 33 buses network without DG presence

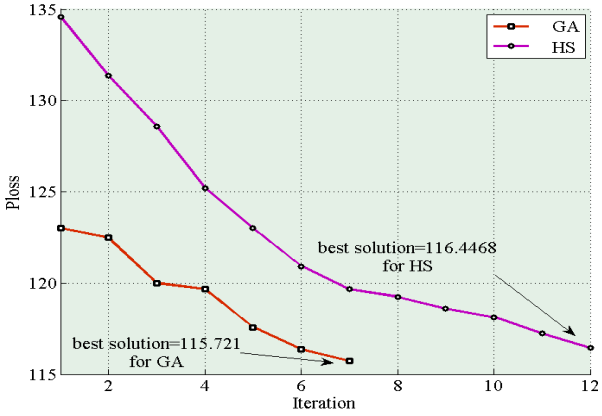

Figure 5. Comparison of the convergence graphs of 2 algorithms for the 33 mesh buses with DG presence

In the second scenario, the grid opt-out option, with the assumption of the constant location of the distributed generation sources (as in Table 2), indicates the network voltage profile in the presence and absence of these resources.

Table 6. 33-Bass Network Voltage Profile Indicator without Distributed Production Resources

	open switch	Voltage profile index	Reduction (%)
initial	s33,s34,s35,s36,s37	0.02984	-
GA	s9,s14,s28,s32,s33	0.01630	45.37
HS	s7,s9,s14,s28,s32	0.01637	45.14

Table 7. 33-Bass network voltage profile index in the presence of distributed generation sources

	open switch	Voltage profile index	Reduction (%)
initial	s33,s34,s35,s36,s37	0.02803	-
GA	s9,s14,s28,s33,s36	0.01525	45.59
HS	s7,s9,s14,s28,s36	0.01573	43.88

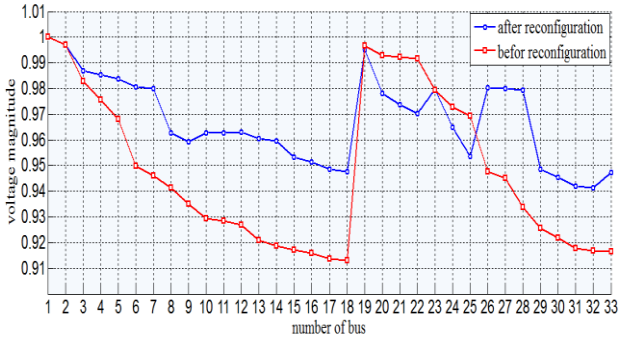

Figure 6. Comparison of network voltage profile of 33 bass before and after rearrangement in the absence of DG

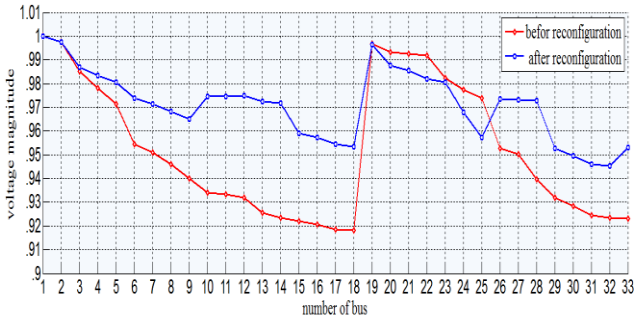

Figure 7. Comparison of network voltage profile of 33 bass before and after rearrangement in the presence of DG

In both cases, the voltage range of most network nodes has increased after rearrangement and closer to 1 per unit, and the whole graph is smoother than before the rearrangement. Second, the voltage range of most nodes has increased significantly compared to the initial arrangement before, after the presence of distributed generation sources, and the comparison of the optimal arrangement before and after the presence of distributed generation sources.

In the third scenario, the effect of the optimal location of distributed generation sources on the reduction of active network losses in the presence of these resources has been studied.

Table 8. The 33-bass network active losses in the DGs primary location and in DGs optimal locations

	The location of DGs	Ploss (kW)	Reduction (%)
Initial	(DG1=3),(DG2=6), (DG3=24),(DG4=29)	169.76	-
GA	(DG1=33),(DG2=18), (DG3=32),(DG4=17)	135.57	20.14
HS	(DG1=33),(DG2=18), (DG3=32),(DG4=17)	135.57	20.14

As you can see, the active power losses in the initial arrangement with the placement of resources in non-optimal locations are 169.66 kW. After applying the optimal location on the network, the genetic algorithm reduces the cascade from 169.76 kW to 135.51 kW, decreasing by 20.14% compared to the initial state. The optimum arrangement with the location of dispersed 1, 2, 3 and 4 generation sources were obtained at places 33, 18, 32 and 17, respectively. The Harmony Search algorithm also has the same function. In the fourth scenario, with the optimal location of dispersed sources of production, the analysis of the voltage profile indicator in the presence of these resources is discussed.

Table 9. The 33-bass network voltage profile index in the DGs primary location and in the DGs optimal location

	The location of DGs	Profile Voltage Index	Reduction (%)
initial	(DG1=3),(DG2=6), (DG3=24),(DG4=29)	0.0280	-
GA	(DG1=32),(DG2=17), (DG3=18),(DG4=16)	0.021656	22.65
HS	(DG1=16),(DG2=17), (DG3=18),(DG4=33)	0.021658	22.65

After optimal positioning on this network, the voltage profile index is significantly improved compared to the initial state. The optimum arrangement with the distribution of dispersed 1, 2, 3 and 4 production sources was obtained at places 32, 17, 18 and 16, respectively. The Harmonic Search algorithm also has a roughly similar function. In the fifth scenario, the active losses and annual net profit of the studied network are investigated after optimal location of the capacitor.

Table 10. The active casualties and the annual profit of the 33 Bass Network after being delivered to the optimal location

	The location of Capacitors	Ploss (kW)	Profit ($)
initial	-	202.5	-
GA	(C1=30),(C2=31), (C3=32),(C4=33)	184.3401	25255.745
HS	(C1=18),(C2=31), (C3=32),(C4=33)	184.6836	24933.2407

After applying the optimum location of the capacitor on the network, the genetic algorithm reduces the losses from 202.5 kW to 184.3401 kW, yielding $ 25,255.745. The optimum arrangement with capacitors 1, 2, 3, and 4 was arranged in places 30, 31, 32 and 33, respectively. The Harmonic Search algorithm has also been shown to function. In the sixth scenario, the voltage profile and the annual profit of the studied network after the optimal location of the capacitor are investigated.

Table 11. Voltage Profile Profit and 33-Bass Annual Network Profit After Optimization

	The location of Capacitors	Voltage Profile Index (kW)	Profit ($)
initial	-	0.02984	-
GA	(C1=16),(C2=18), (C3=15),(C4=17)	0.027611	293776.1576
HS	(C1=16),(C2=17), (C3=14),(C4=18)	0.027631	293776.1282

After optimizing the location on this network, the voltage profile index is significantly improved compared to the initial state. The optimal arrangement with capacitors 1, 2, 3, and 4 was arranged in places 16, 17, 18 and 15, respectively. The Harmonic Search algorithm also has a roughly similar function.

7. CONCLUSION

Genetic algorithm is very suitable for solving this problem due to easy compatibility with discrete variables and having an operator to escape local optimizations. In the case of Harmonic Search Algorithm, it is necessary to spend more time adjusting because the proper adjustment of its parameters is of great importance. Therefore, the incorrect adjustment of these parameters leads to the algorithm's capture in local optimizations or the failure to find the correct answer. Also, the algorithm of Harmonic Search, because it makes the answers in the whole process of performing the variable algorithm into a variable, so an unacceptable response is not generated, and this property has a very high-speed algorithm that if other parameters are set correctly It is very suitable for large networks. While two genetic algorithms produce the answers, they examine the constraints after production. Instead, genetic algorithms, because of their high public search capability, and due to the operator's ability to escape from the local optimization, consider more space at the same time and are less likely to be caught up in local optimizations. But initializing the initial population in the genetic algorithm is very important, and at the time of the convergence of the algorithm and finding the optimal solution is effective. It was also found that the presence of distributed generation resources could be effective in reducing the losses and increasing the voltage range of the various points of the network that dropped.

8. REFERENCES

[1] K. Yousefpour, "Placement of Dispersed Generation with the Purpose of Losses Reduction and Voltage Profile Improvement in Distribution Networks Using Particle Swarm Optimization Algorithm," *Journal of World's Electrical Engineering and Technology*, vol. 2322, p. 5114, 2014.

[2] N. Fahimi, M. R. Chalaki, M. A. Baferani, M. R. Tajik, and A. A. Shayegani, "Investigating the failures of defected silicon rubber insulators in salt-fog chamber," in *Texas Power and Energy Conference (TPEC), 2018 IEEE*, 2018, pp. 1-6.

[3] M. Rostaghi-Chalaki, A. Shayegani-Akmal, and H. Mohseni, "HARMONIC ANALYSIS OF LEAKAGE CURRENT OF SILICON RUBBER INSULATORS IN CLEAN-FOG AND SALT-FOG," in *18th International Symposium on High Voltage Engineering*, 2013, pp. 1684-1688.

[4] M. Rostaghi-Chalaki, A. Shayegani-Akmal, and H. Mohseni, "A STUDY ON THE RELATION BETWEEN LEAKAGE CURRENT AND SPECIFIC CREEPAGE DISTANCE," in *18th International Symposium on High Voltage Engineering (ISH 2013)*, 2013, pp. 1629-1623.

[5] A. Hamedi and M. Ketabdar, "Energy Loss Estimation and Flow Simulation in the skimming flow Regime of Stepped Spillways with Inclined Steps and End Sill: A Numerical Model," *International Journal of Science and Engineering Applications*, vol. 5, pp. 399-407, 2016.

[6] A. Hamedi, "Advanced Characterization of Hydraulic Structures for Flow Regime Control: Experimental Developement," 2017.

[7] P. Dehghanian, S. Aslan, and P. Dehghanian, "Quantifying power system resilience improvement using network reconfiguration," in *IEEE 60th International Midwest Symposium on Circuits and Systems (MWSCAS)*, 2017, pp. 1-4.

[8] H. Pourgharibshahi, M. Abdolzadeh, and R. Fadaeinedjad, "Verification of computational optimum tilt angles of a photovoltaic module using an experimental photovoltaic system," *Environmental Progress & Sustainable Energy*, vol. 34, pp. 1156-1165, 2015.

[9] F. Rahmani, F. Razaghian, and A. Kashaninia, "High Power Two-Stage Class-AB/J Power Amplifier with High Gain and Efficiency," *Journal of Academic and Applied Studies (JAAS)*, vol. 4, pp. 56-68, 2014.

[10] P. Dehghanian, S. Aslan, and P. Dehghanian, "Maintaining Electric System Safety through An Enhanced Network Resilience," *IEEE Transactions on Industry Applications*, 2018.

[11] M. H. Imani, K. Yousefpour, M. J. Ghadi, and M. T. Andani, "Simultaneous presence of wind farm and V2G in security constrained unit commitment problem considering uncertainty of wind generation," in *Texas Power and Energy Conference (TPEC), 2018 IEEE*, 2018, pp. 1-6.
[12] S. Gharghabi and R. Safabakhsh, "Person recognition based on face and body information for domestic service robots," in *Robotics and Mechatronics (ICROM), 2015 3rd RSI International Conference on*, 2015, pp. 265-270.
[13] S. Gharghabi, B. Azari, F. Shamshirdar, and R. Safabakhsh, "Improving person recognition by weight adaptation of soft biometrics," in *Computer and Knowledge Engineering (ICCKE), 2016 6th International Conference on*, 2016, pp. 36-40.
[14] A. Khalili, R. Jha, and N. Jayakody, "Structural Health Monitoring of Skin-Stiffener Structures Using WSFE-based User Defined Elements in Abaqus," in *25th AIAA/AHS Adaptive Structures Conference*, 2017, p. 1677.
[15] M. Montazeri, H. Pourgharibshahi, and M. Mohammadian, "Static voltage stability analysis of IRAN south-east power system using extended CPF method," in *International Power system conference. Tehran-IRAN*, 2012.
[16] S. Shahrokhabadi and M. Toufigh, "The solution of unconfined seepage problem using Natural Element Method (NEM) coupled with Genetic Algorithm (GA)," *Applied Mathematical Modelling*, vol. 37, pp. 2775-2786, 2013.
[17] S. Shahrokhabadi, V. Khoshfahm, and H. N. Rafsanjani, "Hybrid of natural element method (NEM) with genetic algorithm (GA) to find critical slip surface," *Alexandria Engineering Journal*, vol. 53, pp. 373-383, 2014.
[18] M. Khatibi, T. Amraee, H. Zargarzadeh, and M. Barzegaran, "Comparative analysis of dynamic model reduction with application in power systems," in *Power Systems Conference (PSC), 2016 Clemson University*, 2016, pp. 1-6.
[19] F. Rahmani and M. Barzegaran, "Dynamic wireless power charging of electric vehicles using optimal placement of transmitters," in *Electromagnetic Field Computation (CEFC), 2016 IEEE Conference on*, 2016, pp. 1-1.
[20] M. Ketabdar and A. Hamedi, "Intake Angle Optimization in 90-degree Converged Bends in the Presence of Floating Wooden Debris: Experimental Development," *Florida Civ. Eng. J*, vol. 2, pp. 22-27.2016, 2016.
[21] M. Khatibi, H. Zargarzadeh, and M. Barzegaran, "Power system dynamic model reduction by means of an iterative SVD-Krylov model reduction method," in *Innovative Smart Grid Technologies Conference (ISGT), 2016 IEEE Power & Energy Society*, 2016, pp. 1-6.
[22] M. Ketabdar, "Numerical and Empirical Studies on the Hydraulic Conditions of 90 degree converged Bend with Intake," *International Journal of Science and Engineering Applications*, vol. 5, pp. 441-444, 2016.
[23] M. Ketabdar, A. K. Moghaddam, S. A. Ahmadian, P. Hoseini, and M. Pishdadakhgari, "Experimental Survey of Energy Dissipation in Nappe Flow Regime in Stepped Spillway Equipped with Inclined Steps and Sill," *International Journal of Research and Engineering*, vol. 4, pp. 161-165, 2017.
[24] S. H. Imani, S. Asghari, and M. Ameli, "Considering the load uncertainty for solving security constrained unit commitment problem in presence of plug-in electric vehicle," in *Electrical Engineering (ICEE), 2014 22nd Iranian Conference on*, 2014, pp. 725-732.
[25] E. Sadeghian, "Modeling and Checking the Power Quality of High Pressure Sodium Vapor Lamp," 2018.
[26] S. Hashemi, M. Montazeri, and M. Nasiri, "The compensation of actuator delay for hardware-in-the-loop simulation of a jet engine fuel control unit," *Simulation*, vol. 90, pp. 745-755, 2014.
[27] F. Rahmani, F. Razaghian, and A. Kashaninia, "Novel Approach to Design of a Class-EJ Power Amplifier Using High Power Technology," *World Academy of Science, Engineering and Technology, International Journal of Electrical, Computer, Energetic, Electronic and Communication Engineering*, vol. 9, pp. 541-546, 2015.
[28] T. Pourseif, M. T. Andani, Z. Ramezani, and M. Pourgholi, "Model Reference Adaptive Control for Robot Tracking Problem: Design & Performance Analysis," *International Journal of Control Science and Engineering*, vol. 7, pp. 18-23, 2017.
[29] M. T. Andani, H. Pourgharibshahi, Z. Ramezani, and H. Zargarzadeh, "Controller design for voltage-source converter using LQG/LTR," in *Texas Power and Energy Conference (TPEC), 2018 IEEE*, 2018, pp. 1-6.
[30] A. Hamedi, M. Ketabdar, M. Fesharaki, and A. Mansoori, "Nappe Flow Regime Energy Loss in Stepped Chutes Equipped with Reverse Inclined Steps: Experimental Development," *Florida Civil Engineering Journal*, vol. 2, pp. 28-37, 2016.
[31] A. Rouholamini, H. Pourgharibshahi, R. Fadaeinedjad, and M. Abdolzadeh, "Temperature of a photovoltaic module under the influence of different environmental conditions–experimental investigation," *International Journal of Ambient Energy*, vol. 37, pp. 266-272, 2016.
[32] M. Baqersad, M. Mohammadafzali, B. Choubane, C. Holzschuher, A. Hamedi, and H. Ali, "Precision Assessment of the Florida Texture Meter in Hot Mix Asphalt," *Journal of Transportation Engineering, Part B: Pavements*, vol. 144, p. 04018003, 2018.
[33] M. T. Andani and Z. Ramezani, "Robust Control of a Spherical Mobile Robot," 2017.
[34] M. Jafari, G. Atefi, and J. Khalesi, "Advances in nonlinear stress analysis of a steam cooled gas turbine blade," *Latin American applied research*, vol. 42, pp. 167-175, 2012.
[35] M. Hosseini Imani, M. Jabbari Ghadi, S. Shamshirband, and M. M. Balas, "Impact Evaluation of Electric Vehicle Parking on Solving Security-Constrained Unit Commitment Problem," *Mathematical and Computational Applications*, vol. 23, p. 13, 2018.
[36] B. Rahmani and S. R. Hashemi, "Internet-based control of FCU hardware-in-the-loop simulators," *Simulation Modelling Practice and Theory*, vol. 56, pp. 69-81, 2015.
[37] F. K. Purian and E. Sadeghian, "Mobile robots path planning using ant colony optimization and Fuzzy Logic algorithms in unknown dynamic environments," in *Control, Automation, Robotics and Embedded Systems (CARE), 2013 International Conference On*, 2013, pp. 1-6.
[38] S. Shahrokhabadi and A. Ahmadi, "Method of Fundamental Solution (MFS) coupled with Particle Swarm Optimization (PSO) to determine optimal phreatic line in unconned seepage problem," *Scientia Iranica. Transaction A, Civil Engineering*, vol. 20, p. 1327, 2013.
[39] H. N. Rafsanjani, S. Shahrokhabadi, and A. Hadjahmadi, "The Use of Linear Regression to Estimate the Actual

Hourly Production of a Wheel-Type Loader in Construction Projects," in *ICSDEC 2012: Developing the Frontier of Sustainable Design, Engineering, and Construction*, ed, 2013, pp. 727-731.

[40] A. F. Bastani, Z. Ahmadi, and D. Damircheli, "A radial basis collocation method for pricing American options under regime-switching jump-diffusion models," *Applied Numerical Mathematics*, vol. 65, pp. 79-90, 2013.

[41] A. F. Bastani and D. Damircheli, "An adaptive algorithm for solving stochastic multi-point boundary value problems," *Numerical Algorithms*, vol. 74, pp. 1119-1143, 2017.

[42] A. Khalili, R. Jha, and D. Samaratunga, "Spectrally formulated user-defined element in conventional finite element environment for wave motion analysis in 2-D composite structures," *European Journal of Computational Mechanics*, vol. 25, pp. 446-474, 2016.

[43] A. Khalili, D. Samaratunga, R. Jha, T. E. Lacy, and G. Srinivasan, "Wavelet spectral finite element based user-defined element in abaqus for modeling delamination in Composite Beams," in *23rd AIAA/AHS Adaptive Structures Conference*, 2015, p. 1726.

[44] A. Khalili, R. Jha, and D. Samaratunga, "The Wavelet Spectral Finite Element-based user-defined element in Abaqus for wave propagation in one-dimensional composite structures," *Simulation*, vol. 93, pp. 397-408, 2017.

International Journal of Science and Engineering Applications
Volume 7–Issue 06,80-84, 2018, ISSN:-2319–7560

Universal Motor Controller Designing for Washing Machines

David Margaria
Electrical Engineering Department
Zhejiang University, China

Afsoon Bahadoran
Computer Engineering Department
Azad University of Najafabad,
Esfahan, Iran

Abstract: The purpose of this paper is to obtain an accurate system model to test various control schemes for a motion control system that requires high speed, robustness and accuracy. A washing machine equipped with a universal motor is considered. The model of universal motor and its load (washing machine drum) based on the governing mathematical equations is developed in MATLAB-SIMULINK. Using the model, a PID and LQR controller to compensate the effects of disturbance without degrading tracking performance have been designed. In this experiment, it is not preferable for safety reasons to tune the controller online on the actual machinery. The aim of designing the mentioned controllers is rejection of unwanted disturbance caused by laundry position in washing machine; especially the major type of disturbance that occurs in transition mode. Finally, the simulation results of both controllers are compared.
Keywords: PID; LQR; Controller; Washing Machine; Universal Motor.

1. INTRODUCTION

In home appliances and light household equipment, electronics is commonly found in the man machine interface (dashboards, control panels, remote controls, etc...), as well as in the management of complex operating sequences, such as in washing machines; however, it is only just beginning to be used to control the electric motors which power them with high efficiency [1].

Energy saving, silence, flexibility and simplicity are requirements of growing importance: in applications such as drills, washing machines, vacuum-cleaners and refrigerators, variable speed control is the principal means of obtaining such performance features. Many motors are to be found in the various items of domestic equipment in a typical home. This illustrates the important role that electronics is bound to play in the control of home appliance motors.

Universal motors are widely used in household appliances like washing machine, vacuum cleaners, sewing machines and most domestic appliances because it is cost effective in respect of volume/power and it has a good torque response. In the control of these motors, generally, providing stable speed control, preventing large currents and drawing minimum harmonic current from ac mains supply are required. To meet these requirements using AC chopper with current and speed feedback is preferred. In addition, a control system with low cost is desired. To maintain the motor speed as the load varies, the application must control the voltage applied to the motor by either “phase angle modulation” techniques.

In the field of washing machine speed control the major challenge is inconstant applied torque to motor. Unpredictable place of laundry in washing machine results in disturbance of applied torque to motor. In addition, in transition mode from wash to dehydration (spin) change in position of laundry in drum results in sudden high changes in torque. Lee et. al tries to estimate the laundry moment of inertia in different washing stages in order to optimize the washing time by real time test equipments [2, 3].

Since, different types of motor are being utilized in washing machines, different controlling methods are reviewed for each motor type. Vaclavek and Blaha proposed Lyapanov function based for AC induction motor control Chi and Xu suggested sliding-mode [4, 5] sensorless control for direct drive washing machine motors [6, 7]. In some other application fuzzy logic controlling method is used [8, 9]. In this research, a universal motor is going to be controlled. Universal motors are the most common motors in washing machines because of low cost and high start torque. In this paper, both PID and LQR controlling are proposed for washing machine control [10].

This paper presents the experimental and theoretical studies of universal motors for washing machines. The mathematical model of the universal motor and its load (drum) in washing machine is formed at first and MATLAB-SIMULINK model is developed. This model uses the electromechanical parameters of the motor and drum. Using the model, a PID and LQR and adaptive controller [11]to compensate the effects of disturbance without degrading tracking performance have been designed. In this experiment, it is not preferable for safety reasons to tune the controller online on the actual machinery. Experimental results confirm that the model is a good approximation of washing machine dynamics and the proposed control methodology is effective. Finally, the simulation results of both controllers are compared.

2. LOAD MODELING

Main driving parts of washing machine includes motor, power transmission system (pulley & shaft) and drum. Clothes in washing machine are washed via rotation of drum. All rotating parts are assembled in tub which is connected to washing machine structure by a suspension system which contains some springs and dampers. Figure 1 demonstrates washing machine main inner parts.

Each washing cycle of washing machine includes at least three main steps: washing, rinsing and spinning. The purpose of wash is removing dirt and soils from clothes. Therefore, in real time tests, clothes must be fallen from specific height in order to achieve maximum washing performance [12].

The purpose of rinsing cycle is removing detergent from clothes. Similarly, rinsing cycles requires 45 rpm rotation speed. After wash and rinse mode washing machine starts

dehydration mode. Due to the fact that dehydration cycle uses centrifugal force for removing wet from clothes, it requires high rotation speeds. Usual spinning speeds for dehydration is around 1000 rpm.

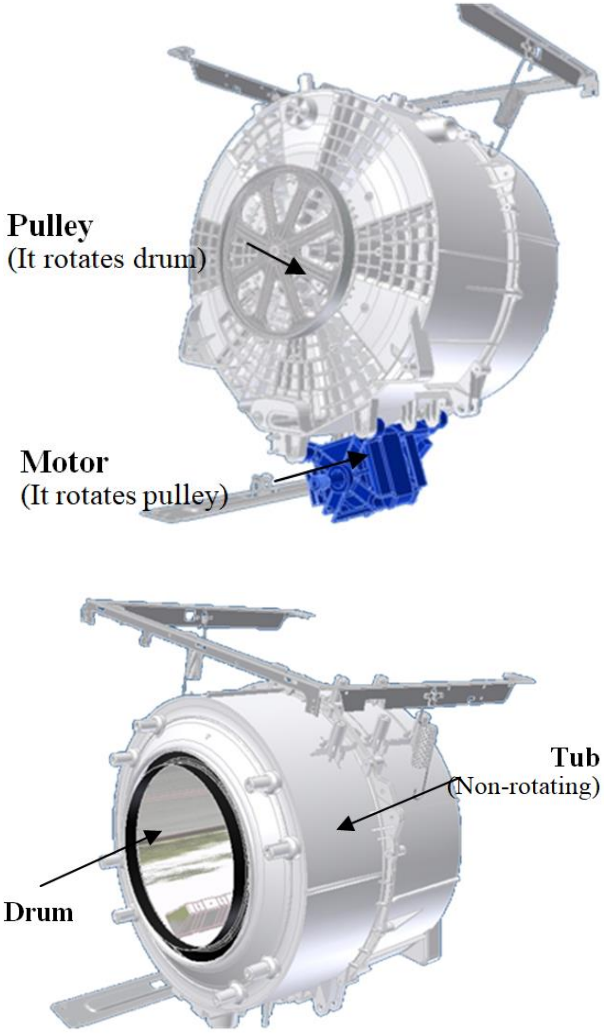

Figure 1. Inner parts of a horizontal washing machine.

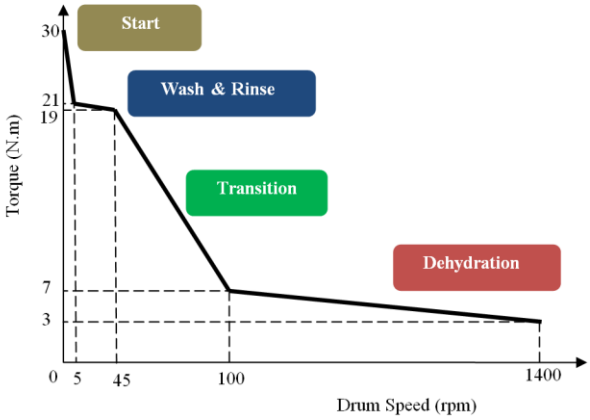

Figure 2. Typical diagram of torque changes in different modes of washing.

High viscosity between the drum and the laundry, force caused by falling laundry, and different moment of inertia are the main reasons which results in sudden torque changes while washing mode are changing to dehydration mode. Schematically, torque versus drum speed diagram is presented in Figure 2. Numbers in this figure are typical and differ regarding the amount of clothes in washing machine and washing machine structure. Therefore, a proper controller must be designed to reject the torque variation in the real time close loop of washing machine system.

Main challenges in motor speed control challenges are caused because of the following points [13, 14]:

1- Sudden torque changes in transition mode.
2- The exact mass of laundry in washing machine put by customer is not predictable. In other words, an operator may put 1 to 7 kg clothes in a 7 kg washing machine.
3- Exact position of laundry in washing machine drum cannot be determined.

3. MATHEMATICAL MODEL

The mathematical model of the universal motor and its load (drum) in washing machine is formed at first and MATLAB-SIMULINK model is developed. This model uses the electromechanical parameters of the motor and drum as follow. Figure 3 demonstrates mechanical model of universal motor in washing machine.

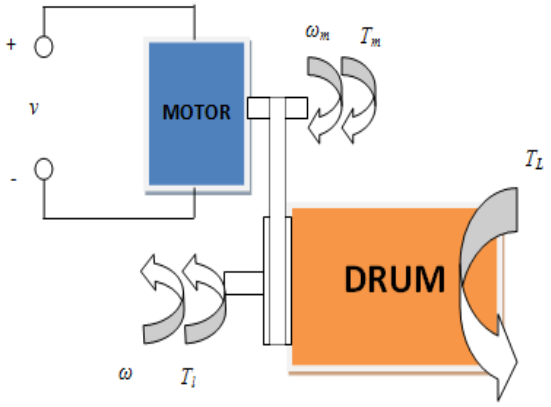

Figure 3- the schematic of motor and washing machine drum.

As shown in Figure 3, the motor and drum are linked by a belt and pulley. Applying Newton's second low to the rotor,

$$J_m\dot{\omega}_m = T_m - T_l \quad (1)$$

Where TL is the torque exerted on the motor shaft by the load, transmitted through the belt. So the torque at the motor shaft is seen to be the torque generated by the motor, minus the torque required to accelerate the motor. The torque exerted by the motor on the load shaft, transmitted through the pulley, is NT_l. Newton's second low applied to the drum is

$$J\dot{\omega} = NT_m - T_L - NJ_m\dot{\omega}_m \quad (2)$$

Since , this becomes

$$(J + N^2 J_m)\dot{\omega} = NT_m - T \quad (3)$$

$$J_e = J + N^2 J_m \quad (4)$$

where J_e is effective inertia seen at the load shaft.

$$T_m = K_a i_a \quad (5)$$

So

$$\dot{\omega} = \frac{NK_a}{J_e} i_a - \frac{T_L}{J_e} \quad (6)$$

To find the transfer function for the block diagram of the open and closed loop system a differential equation to describe the system dynamic. Kirchhoff's voltage is use to map the armature circuitry dynamic of the motor.

$$L_a \frac{di_a}{dt} + r_a i_a = v - K_b \omega_m \quad (7)$$

From the transfer function, the block diagram of the motor and its load is illustrated by Figure 4.

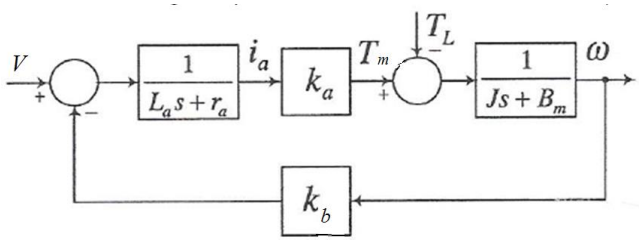

Figure 4. Block Diagram of the Universal Motor

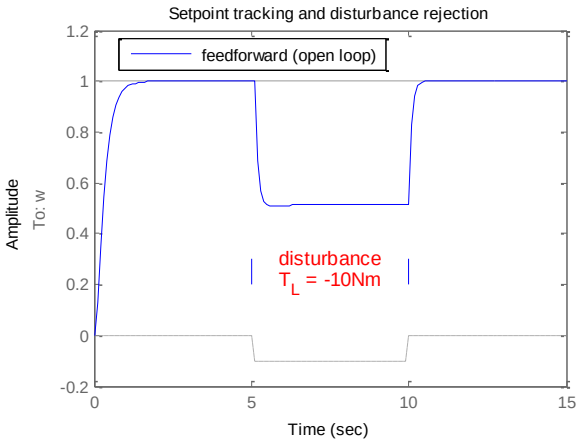

Figure 5. Open loop step response in peresence of a determined load (10 Nm)

To evaluate the feedforward design in the face of load disturbances, the response to a step command w_ref=1 with a disturbance T_d = -10 Nm between t=5 and t=10 seconds is depicted in Figure 5. This disturbance occurs in transition stage regarding to Figure 2. According to the response designing a proper controller for this system is inevitable.

4. PID Controller

PID Control (proportional-integral-derivative) is by far the widest type of automatic control used in industry. Even though it has a relatively simple algorithm/structure, there are many subtle variations[15] in how it is applied in industry. A proportional–integral–derivative controller (PID controller) is a generic control loop feedback mechanism widely used in industrial control systems [16, 17]. A PID controller will correct the error between the output and the desired input or set point by calculating and give an output of correction that will adjust the process accordingly. A PID controller has the general form

$$v(t) = K_p e(t) + K_i \int_0^t e(\tau)d\tau + K_d \frac{de}{dt} \quad (8)$$

Where K_p is proportional gain, K_i is the integral gain, and K_d is the derivative gain. The PID controller calculation (algorithm) involves three separate parameters; the Proportional, the Integral and Derivative values. The Proportional value determines the reaction to the current error, the Integral determines the reaction based on the sum of recent errors and the Derivative determines the reaction to the rate at which the error has been changing [16]. The weighted sum of these three actions is used to adjust the process via a control element such as the position of a control valve, the power supply of a heating element or universal speed and position through an intelligent hardware in the loop experiment setup [18].

Using the linear PID controller from the block diagram developed and documented in Figure 4, it obtains the closed loop system illustrated in Figure 6.

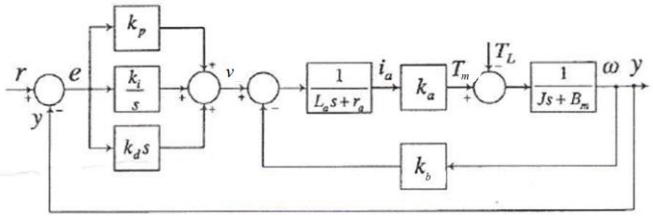

Figure 6. Block Diagram of the Closed-Loop Servo with PID Controller

5. Linear Quadratic Regulator (LQR) Algorithm

The advantages of used LQR are it is easy to design and increases the accuracy of the state variables by estimating the state. The nice feature of the LQR control as compared to pole placement is that instead of having to specify where n eigenvalues should be placed a set of performance weighting are specified that could have more intuitive appeal. The result is a control that is guaranteed to be stable and the output of the circuit is very acceptable [19].

In layman's terms, Linear Quadratic Regulator (LQR) means the settings of a (regulating) controller governing either a machine or process (like an airplane or chemical reactor) are

found by using a mathematical algorithm that minimizes a cost function with weighting factors supplied by a human (engineer). The "cost" (function) is often defined as a sum of the deviations of key measurements from their desired values. In effect this algorithm therefore finds those controller settings that minimize the undesired deviations, like deviations from desired altitude or process temperature. Often the magnitude of the control action itself is included in this sum as to keep the energy expended by the control action itself limited [20, 21].

In the particular case of a quadratic performance index combining the square of the error and square of the actuation, the solution to the optimal control problem is a feedback control where the measurements used for the feedback are all of the state variables. In this feedback control, each of the state variables is multiplied by a gain and the results are summed to get a single actuation value. The result of the LQR formulation is the set of gains, based on the relative weighting of the error and actuation in the performance index.

In addition to the integral of error, the LQR scheme also uses the state vector $x=(i_a,\omega_a)$ to synthesize the driving voltage V, as shown in Figure 8. The resulting voltage is of the form

$$v = K_1 * \omega + K_2 * \omega / s + K_3 * i_a \quad (9)$$

For better disturbance rejection, a cost function that penalizes large integral error is used. The cost function is,

$$C = \int_0^\infty (20q(t)^2 + \omega(t)^2 + 0.01v(t)^2)dt \quad (10)$$

$$q(s) = \omega(s) / s. \quad (11)$$

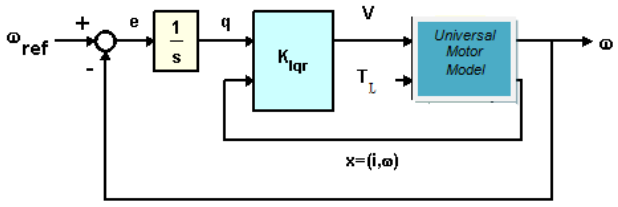

Figure 7. Block Diagram of the Closed-Loop Servo with LQR Controller

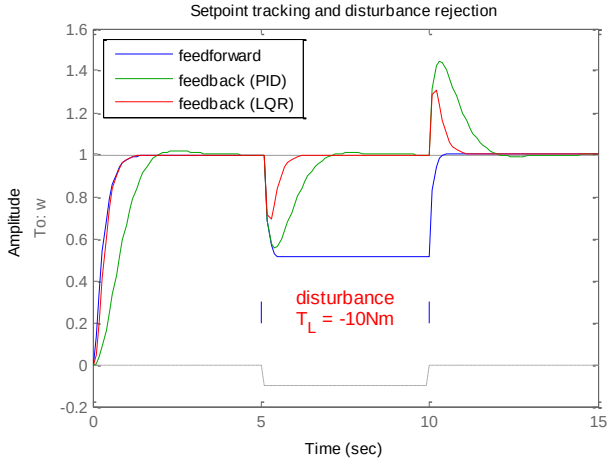

Figure 8. Open loop step response in peresence of a determined load (10 Nm)

To evaluate the PID and LQR controller design in the face of load disturbances, the response to a step command w_ref=1 with a disturbance Td = -10Nm between t=5 and t=10 seconds is simulated as shown in Figure 8.

6. Conclusions

In this paper, The model of universal motor and its load (washing machine drum) based on the governing mathematical equations is developed in MATLAB-SIMULINK. Then, a proper PID and LQR controller were proposed based on the desired response. To test these designed controller on unwanted disturbance caused by drum, a load exerted on system. The results as shown in Figure 8 , confirm that the PID controller cannot trace the set point as good as LQR controller can.

Nomenclature

V	Voltage
ωm	Motor Speed
Tm	Motor Torque
ω	Drum Speed
TL	Load
ia	Current
J	Drum moment of inertia
Kb	Back emf constant
Ka	Motor constant
ra	Resistance
La	Inductance
Jm	Motor moment of inertia

7. REFERENCES

[1] F. Rahmani, F. Razaghian, and A. Kashaninia, "Novel Approach to Design of a Class-EJ Power Amplifier Using High Power Technology," *World Academy of Science, Engineering and Technology, International Journal of Electrical, Computer, Energetic, Electronic and Communication Engineering*, vol. 9, pp. 541-546, 2015.

[2] J.-H. Lee, C.-H. Hwang, K.-m. Kim, W.-C. Lee, C.-Y. Won, and Y.-R. Kim, "Optimal washing time control algorithm for the drum washing machine using an inertia estimator," in *Power and Energy Conference, 2008. PECon 2008. IEEE 2nd International*, 2008, pp. 1393-1398.

[3] S. Hashemi, M. Montazeri, and M. Nasiri, "The compensation of actuator delay for hardware-in-the-loop simulation of a jet engine fuel control unit," *Simulation*, vol. 90, pp. 745-755, 2014.

[4] P. Vaclavek and P. Blaha, "Lyapunov function based flux and speed observer for ac induction motor sensorless control implementation on motorola dsp," in *Industrial Technology, 2003 IEEE International Conference on*, 2003, pp. 536-541.

[5] M. T. Andani and Z. Ramezani, "Robust Control of a Spherical Mobile Robot," 2017.

[6] S. Chi, Z. Zhang, and L. Xu, "Sliding-mode sensorless control of direct-drive PM synchronous motors for washing machine applications," *IEEE Transactions on Industry Applications*, vol. 45, pp. 582-590, 2009.

[7] K. Yousefpour, "Placement of Dispersed Generation with the Purpose of Losses Reduction and Voltage Profile Improvement in Distribution Networks Using Particle Swarm Optimization Algorithm," *Journal of World's Electrical Engineering and Technology*, vol. 2322, p. 5114, 2014.

[8] P. Guillemin, "Fuzzy logic applied to motor control," *IEEE transactions on industry applications*, vol. 32, pp. 51-56, 1996.

[9] H. Pourgharibshahi, M. Abdolzadeh, and R. Fadaeinedjad, "Verification of computational optimum tilt angles of a photovoltaic module using an experimental photovoltaic system," *Environmental Progress & Sustainable Energy*, vol. 34, pp. 1156-1165, 2015.

[10] M. T. Andani, H. Pourgharibshahi, Z. Ramezani, and H. Zargarzadeh, "Controller design for voltage-source converter using LQG/LTR," in *Texas Power and Energy Conference (TPEC), 2018 IEEE*, 2018, pp. 1-6.

[11] T. Pourseif, M. T. Andani, Z. Ramezani, and M. Pourgholi, "Model Reference Adaptive Control for Robot Tracking Problem: Design & Performance Analysis," *International Journal of Control Science and Engineering*, vol. 7, pp. 18-23, 2017.

[12] B. Rahmani and S. R. Hashemi, "Internet-based control of FCU hardware-in-the-loop simulators," *Simulation Modelling Practice and Theory*, vol. 56, pp. 69-81, 2015.

[13] A. Rouholamini, H. Pourgharibshahi, R. Fadaeinedjad, and G. Moschopoulos, "Optimal tilt angle determination of photovoltaic panels and comparing of their mathematical model predictions to experimental data in Kerman," in *Electrical and Computer Engineering (CCECE), 2013 26th Annual IEEE Canadian Conference on*, 2013, pp. 1-4.

[14] M. Jafari, G. Atefi, J. Khalesi, and A. Soleymani, "A new conjugate heat transfer method to analyse a 3D steam cooled gas turbine blade with temperature-dependent material properties," *Proceedings of the Institution of Mechanical Engineers, Part C: Journal of Mechanical Engineering Science*, vol. 226, pp. 1309-1320, 2012.

[15] A. Mohammed, M. Alhadri, W. Zakri, and H. Aliniagerdroudbari, "Design and Comparison of Cooling Plates for a Prismatic Lithium-ion Battery for Electrified Vehicles," *SAE Technical Paper*, pp. 01-1188, 2018.

[16] J. Tang, "PID controller using the TMS320C31 DSK with online parameter adjustment for real-time DC motor speed and position control," in *Industrial Electronics, 2001. Proceedings. ISIE 2001. IEEE International Symposium on*, 2001, pp. 786-791.

[17] M. H. Imani, K. Yousefpour, M. J. Ghadi, and M. T. Andani, "Simultaneous presence of wind farm and V2G in security constrained unit commitment problem considering uncertainty of wind generation," in *Texas Power and Energy Conference (TPEC), 2018 IEEE*, 2018, pp. 1-6.

[18] S. R. Hashemi and M. Montazeri-Gh, "Polynomial-based time-delay compensation for hardware-in-the-loop simulation of a jet engine fuel control unit," *International Journal of Automation and Control*, vol. 8, pp. 323-338, 2014.

[19] F. Rahmani, F. Razaghian, and A. Kashaninia, "High Power Two-Stage Class-AB/J Power Amplifier with High Gain and Efficiency," *Journal of Academic and Applied Studies (JAAS)*, vol. 4, pp. 56-68, 2014.

[20] R. C. Nelson, *Flight stability and automatic control* vol. 2: WCB/McGraw Hill New York, 1998.

[21] B. Etkin and L. D. Reid, *Dynamics of flight: stability and control* vol. 3: Wiley New York, 1996.

International Journal of Science and Engineering Applications
Volume 7–Issue 06,85-93, 2018, ISSN:-2319–7560

Investigation of Ride Quality of the Truck Using Sinusoidal Road Pavement in Low and High Speed by Utilizing Lagrange Method

Ali Rahmani
Assistant Professor,
Department of Mechanical and Materials Engineering
Shahid Rajaee Teacher Training University,
Tehran, Iran

Pedram Hoseini
MSc Student
Department of Mechanical Engineering
Amirkabir University of Technology
Tehran, Iran

Abstract: In this research, ride quality of a truck is investigated to understand vibration specifications of the multi-degree of freedom 3-axle rigid truck. for this purpose, a Benz 2624 model have been modelled. An off-road duty is considered for this analysis. A modeling procedure and simulation of the truck is produced in this research. The system is modelled by a linear model which contains the seat and cab suspensions, rigid live axles, and also suspension geometries, the motion equations and system matrices are obtained by utilizing the Lagrange's equation. Then, a numerical central difference method is utilized to gain the system responses subject to the sinusoidal road excitations. Truck's physical parameters and dynamic properties of its components are not well-known therefore these properties have been achieved by modeling the truck in SOLIDWORKS software. Finally, a code based on these equations is developed in MATLAB software to calculate system time responses under different cases, which contains low and high drive frequency of the truck. The developed model can also be used for newer trucks with some modifications to change the current model it's necessary to have accurate information for input data.

Keywords: Multi-axles truck, Lagrange equations, Road excitations, Vibration analysis, System response

1. INTRODUCTION

Modeling procedure is an important part in engineering. The two types of the modeling are: Numerical and physical modeling, which used widely in engineering [1-12]. Vibration modeling is one of the applications for modeling and analyzing in engineering. For example, Vibration has an important role in design and maintenance of bridge structures especially when the frequency is close to bridge's natural vibrations [13-14]. Many fields and products like, e.g., aerospace [15-19], automobile, transportation, satellite with high frequency switches, electric vehicle, buildings, and so on have been improved by the contribution of vibration analysis [20]. Identification and suppression of unwanted vibrations are the most common goal to improve product quality. As a real-world example, Multi-axel truck need this procedure to breakdown its vibrations.

Dynamic excitation causes by the interaction between vehicle's wheels and road surface. Different vibration levels occur by the amount of elevation of the road surface unevenness and the vehicle's speed [21-22]. Heavy vehicles produce the most perceptible vibrations. A vehicle model is used to describe the dynamic behavior of the vehicle, which is consisted of discrete masses, springs, friction elements and dampers [23-27]. By obtaining a linear model of a vehicle with high output and acceptable efficiency, the calculation of axle loads is facilitated by using Frequency Response Functions [28]. Local road unevenness is expressed by utilizing deterministic function, which is showing the deviation of the travelled surface from a true planar surface. By the utilizing a Power Spectral Density the global road unevenness can also be defined in a stochastic way [29-35].

Many models such as quarter, bicycle, half and full models of vehicle have been investigated with different numbers of DoF for vehicle dynamics [36-41]. One of the most famous models for vehicles is Eight-DoF model, including forward, lateral, yaw and roll motion and four DoF for travel of each wheel [30]. In the literature, multibody system dynamic models of vehicles have also been proposed. For instance, Rahmani Hanzaki et al. proposed a methodology for dynamic analysis of a multibody system with spherical joints. As an example, for that they have considered a suspension system of a vehicle [31]. Applying this methodology to a three-axle truck makes complicated computation. Therefore, other discrete model for the truck has been employed. For example, Tabatabaee developed a 16-DoF non-linear model an articulated vehicle, which is validated experimentally [32].

In this paper a survey on the equations of motion will be presented, by the use of Lagrange equation, to finally determine system responses of a complete 3-D rigid three-axle truck model subject to sinusoidal road excitations, in different cases and different speeds. This analysis can be useful to better understand the coupled motions of the truck's wheels. The validation of equations has been verified by utilizing ADAMS software in our previous paper [33-35]. The developed 19 DoF model can be used for other trucks by applying changes in material properties and adding estimations. Mathematical modeling that was discussed in Zeidi et al. [36-41] is continued in the present study for discretization of 19 DOF truck. Impact of CO emission, which was discussed in Aghaei et al. [42], has also been used in the current model as input for the current model.

2. MODELING THE TRUCK

Experimental methods are the most reasonable techniques to acquire mass properties of components of a manufactured vehicle, but these techniques are very costly. Therefore, for this work, to obtain masses, centers of mass, moments of inertia etc. of the three-axle truck a SOLIDWORKS model of the vehicle have been modeled and utilized. For dynamic simulation of the truck these physical properties are highly

necessary. Figures 1 and 2 shows two views of the assembled truck model, and some of the trucks components are depicted, respectively. In modelling this truck, the weighty components are modeled precisely, such as chassis, cabin, differentials, tires, springs etc. Non-homogeneous material is assigned to this model since differential consists of several material and precision of properties, which are acquired from this model are more acceptable.

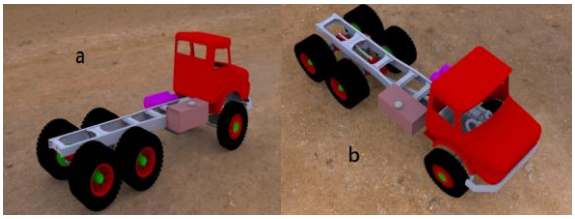

Figure 1. CAD model of the three-axle truck

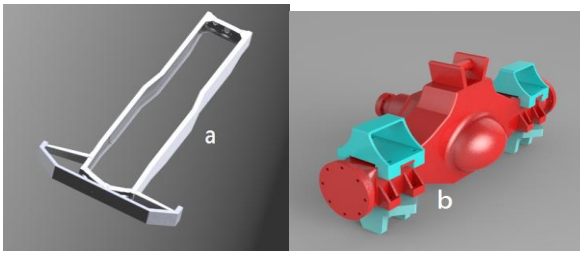

Figure 2. Two main CAD modelled components of the truck; a) chassis, b) axle with differential

2.1 Governing the Equations

The Lagrange method is utilized to obtain dynamic behavior of the mentioned three-axle truck. 19-DoF mathematical model is considered for the truck. M1, M2 and M3 are the axles of the truck as shown in Figure 3. Blue springs are considered on behalf of tires and red springs as leaf springs of the suspensions systems. Green springs are counted for connecting cabin to the frame and finally, purple spring is used to suspend driver's seat with respect to the cabin. As the rests, W, θ, and φ illustrate displacement, roll, and pitch of the truck in this dynamic analysis. Hence, the 19 DoFs are as follow:

- Driver seat bounce, one degree; w_106;
- Cab bounce, pitch and roll, three degrees; orderly w_104, θ_104, φ_104;
- Chassis bounce (sprung mass), pitch and roll, three degrees; w_100, φ_100, θ_100, respectively:
- Front axle, its bounce and roll, two degrees; orderly w_101, θ_101;
- Intermediate axle, bounce and roll, two degrees; orderly w_102 , θ_102;
- Rear axle, bounce and roll, two degrees; orderly w_103, θ_103;
- 6 bounce motion of the 6 wheels; w_1, w_2, w_3, w_4, w_5, w_6; where w_1 and ; w_2are the bounce of left and right steer wheels, respectively; w_3 and w_4 are the bounce of left and right wheels of the middle axle, correspondingly; w_5 and w_6are the bounce of left and right wheels of rear axle, respectively.

The vector of coordinates for the vehicle is written as:

W_19=[w_106 w_104 θ_104 φ_104 〖w〗_(100 θ_100) φ_100 w_101 θ_101 w_102 θ_102 w_103 θ_103 w_1 w_2 w_3 w_4 w_5 w_6]^T

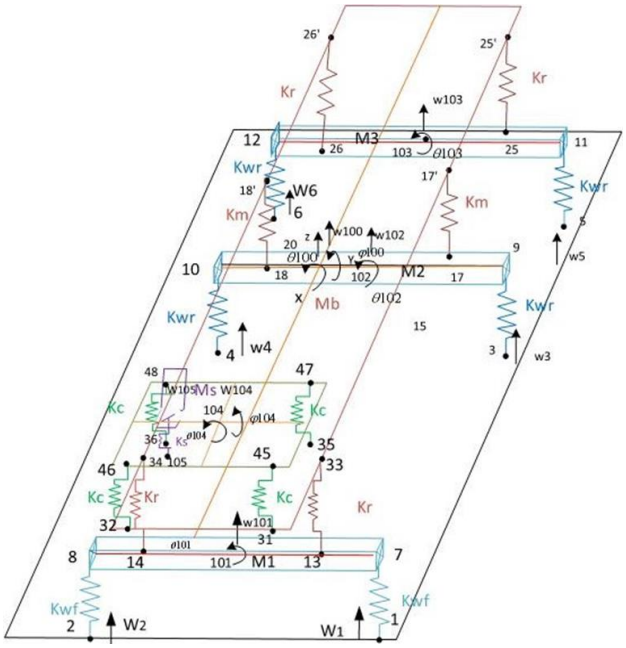

Figure 3. The scheme of the 19-DoF model for the truck

Figure 4(a) shows truck model in X-Z plane and distances between different important points. In addition, Figure 4(b) indicates the model in Y-Z plane and the related parameters.

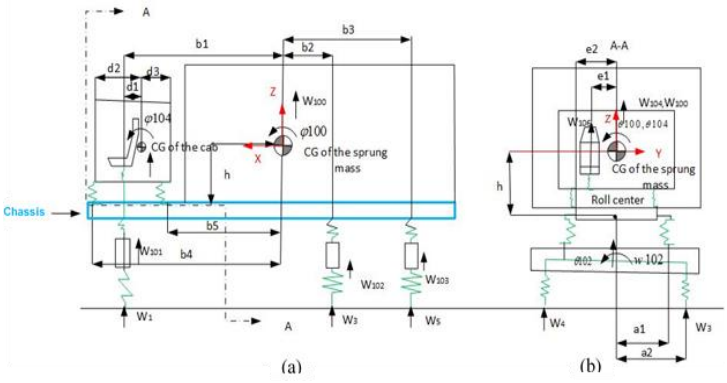

Figure 4. CGs (Center of gravity) and other essential parameters of the truck.

2.2 Motion Equations

The well-known Lagrange equation for this system is in the following form:

$$\frac{d}{dt}\left(\frac{dT}{d\dot{W}_{19}}\right)-\left(\frac{dT}{dW_{19}}\right)+\left(\frac{dP}{dW_{19}}\right)+\left(\frac{dR}{d\dot{W}_{19}}\right)=0 \qquad (2)$$

Where T, P and R are the kinematic, potential and dissipation energies of the system, respectively.

The kinetic energy part of the system is obtained as:

$$\begin{aligned}T=&\tfrac{1}{2}M_s(\dot{W}106)^2+\tfrac{1}{2}M_c(\dot{W}104)^2+\\&\tfrac{1}{2}M_b(\dot{W}100)^2+\tfrac{1}{2}M_1(\dot{W}101)^2+\tfrac{1}{2}M_2(\dot{W}102)^2+\\&\tfrac{1}{2}M_3(\dot{W}103)^2+\tfrac{1}{2}I_{cx}(\dot{\theta}104)^2+\tfrac{1}{2}I_{bx}(\dot{\theta}100)^2+\\&\tfrac{1}{2}I_{1x}(\dot{\theta}101)^2+\tfrac{1}{2}I_{2x}(\dot{\theta}102)^2+\tfrac{1}{2}I_{3x}(\dot{\theta}103)^2+\\&\tfrac{1}{2}I_{cy}(\dot{\theta}104)^2+\tfrac{1}{2}I_{by}(\dot{\theta}100)^2\end{aligned} \qquad (3)$$

Moreover, the potential energy part of the system is as follow:

$$\begin{aligned}P=&\tfrac{1}{2}K_s(W106-W105)^2+\tfrac{1}{2}K_c(W45-W31)^2+\\&\tfrac{1}{2}K_c(W46-W32)^2+\tfrac{1}{2}K_c(W47-W35)^2+\\&\tfrac{1}{2}K_c(W48-W36)^2+\tfrac{1}{2}K_f(W33-W13)^2+\\&\tfrac{1}{2}K_f(W34-W14)^2+\tfrac{1}{2}K_m(W17`-W17)^2+\\&\tfrac{1}{2}K_m(W18`-W18)^2+\tfrac{1}{2}K_r(W25`-W25)^2+\\&\tfrac{1}{2}K_r(W26`-W26)^2+\tfrac{1}{2}K_{Wf}(W7-W1)^2+\\&\tfrac{1}{2}K_{Wf}(W8-W2)^2+\tfrac{1}{2}K_{Wr}(W9-W3)^2+\\&\tfrac{1}{2}K_{Wr}(W10-W4)^2+\tfrac{1}{2}K_{Wr}(W11-W5)^2+\\&\tfrac{1}{2}K_{Wr}(W12-W6)^2\end{aligned} \qquad (4)$$

And the dissipation energy part of the system is:

$$\begin{aligned}R=&\tfrac{1}{2}c_s(\dot{W}106-\dot{W}105)^2+\tfrac{1}{2}c_{c1}(\dot{W}45-\\&\dot{W}31)^2+\tfrac{1}{2}c_{c2}(\dot{W}46-\dot{W}32)^2+\tfrac{1}{2}c_{c3}(\dot{W}47-\\&\dot{W}35)^2+\tfrac{1}{2}c_{c4}(\dot{W}48-\dot{W}36)^2+\tfrac{1}{2}c_1(\dot{W}33-\dot{W}13)^2+\\&\tfrac{1}{2}c_2(\dot{W}34-\dot{W}14)^2+\tfrac{1}{2}c_{s3}(\dot{W}17`-\dot{W}17)^2+\\&\tfrac{1}{2}c_{s4}(\dot{W}18`-\dot{W}18)^2+\tfrac{1}{2}c_{s5}(\dot{W}25`-\dot{W}25)^2+\\&\tfrac{1}{2}c_{s6}(\dot{W}26`-\dot{W}26)^2\end{aligned} \qquad (5)$$

The equations of motion can be organized by differentiating of T, P and R with respect to the coordinates and time according to eq. (2), this gives:

$$M.\ddot{W}+C.\dot{W}+K.W=0 \qquad (6)$$

In which M_{19}, K_{19} and C_{19} are mass matrix, stiffness matrix and damping matrix of the 19 DoF of the truck-poster system model, respectively. In this equation, $\ddot{W}_{19}$, $\dot{W}_{19}$ and W_{19} are acceleration vector, velocity vector and displacement vector of the 19 DoF truck model. In addition, the diagonal system mass matrix, M_{19}, is calculated as follow:

$$M_{19}=\mathrm{diag}[M_s\ M_c\ I_{cx}\ I_{cy}\ M_b\ I_{bx}\ I_{by}\ M_1\ I_{1x}\ M_2\ I_{2x}\ M_3\ I_{3x}\ M_{01}\ M_{02}\ M_{03}\ M_{04}\ M_{05}\ M_{06}]$$

Where, "diag" illustrates that the M_{19} matrix is diagonal; M_s to M_{06} are located on the main diagonal of this matrix. In this relation, M_s and M_c are masses of the seat and the driver, and the cab, respectively; I_{cx} and I_{cy} are inertia of the cab about X and Y axes, correspondingly. In the following, M_b, I_{bx}, and I_{by} point to sprung mass, inertia of the sprung mass about X and Y axes, respectively; Also, 1, 2, and 3 as the indexes in order point to the front axle, middle axle, and the rear axle of the truck. Similarly, M_{01} to M_{06} shows the masses of the front left to rear right wheels, as well. The 19 nonzero values have been achieved from the truck model in Solidworks software by utilizing mass properties. Now, the system damping matrix and stiffness matrix can be written in the following form:

$$C_{19}=\begin{bmatrix}C_{1,1}&C_{1,2}&\cdots&C_{1,19}\\C_{2,1}&C_{2,2}&&C_{2,19}\\\vdots&&\ddots&\vdots\\C_{19,1}&C_{19,2}&\cdots&C/_{19,19}\end{bmatrix},\qquad K_{19}=\begin{bmatrix}K_{1,1}&K_{1,2}&\cdots&K_{1,19}\\K_{2,1}&K_{2,2}&&K_{2,19}\\\vdots&&\ddots&\vdots\\K_{19,1}&K_{19,2}&\cdots&K_{19,19}\end{bmatrix}$$

The non-zero components of C_{19} and K_{19} are as following:

$$\begin{aligned}&C_{1,1}=C_s,\ C_{1,2}=C_{2,1}=-C_s,\ C_{1,3}=C_{3,1}=C_s.e_1,\\&C_{1,4}=C_{4,1}=C_s.d_1\\&C_{2,2}=C_s+C_{c1}+C_{c2}+C_{c3}+C_{c4},\\&C_{2,3}=C_{3,2}=-C_s.e_1+C_{c1}.e_2-C_{c2}.e_2+C_{c3}.e_2-\\&C_{c4}.e_2\\&C_{2,4}=C_{4,2}=-C_s.d_1-C_{c1}.d_2-C_4.C_2.d_2+C_{c3}.d_3+\\&C_{c4}.d_3\\&C_{2,5}=C_{5,2}=-C_{c1}-C_{c2}-C_{c3}-C_{c4},\\&C_{2,6}=C_{6,2}=C_{3,5}=C_{5,3}=-C_{c1}.e_2+C_{c2}.e_2-\\&C_{c3}.e_2+C_{c4}.e_2\\&C_{2,7}=C_{7,2}=C_{c1}.b_4+C_{c2}.b_4+C_{c3}.b_5+C_{c4}.b_5;\\&C_{3,3}=C_s.e_1^2+C_{c1}.e_2^2+C_{c2}.e_2^2+C_{c3}.e_2^2+C_{c4}.e_2^2,\\&C_{3,4}=C_{4,3}=C_s.d_1.e_1-C_{c1}.d_2.e_2+C_{c2}.d_2.e_2+\\&C_{c3}.d_3.e_2-C_{c4}.d_3.e_2\\&C_{3,6}=C_{6,3}=-C_{c1}.e_2^2-C_{c2}.e_2^2-C_{c3}.e_2^2-C_{c4}.e_2^2,\\&C_{3,7}=C_{7,3}=C_{c1}.b_4.e_2-C_{c2}.b_4.e_2+C_{c3}.b_5.e_2-\\&C_{c4}.b_5.e_2\end{aligned}$$

$C_{4,4} = C_s.d_1^2 + C_{c1}.d_2^2 + C_{c2}.d_2^2 + C_{c3}.d_3^2 + C_{c4}.d_3^2,$
$C_{4,5} = C_{5,4} = C_{c1}.d_2 + C_{c2}d_2 - C_{c3}.d_3 - C_{c4}.d_3,$

$C_{4,6} = C_{6,4} = C_{c1}.d_2.e_2 - C_{c2}.d_2.e_2 - C_{c3}.d_3.e_2 + C_{c4}.d_3.e_2$
$C_{4,7} = C_{7,4} = -C_{c1}.b_4.d_2 - C_{c2}.b_4.d_2 + C_{c3}.b_5.d_3 + C_{c4}.b_5.d_3;$

$C_{5,5} = C_{c1} + C_{c2} + C_{c3} + C_{c4} + C_1 + C_2 + C_3.l_2^2/l_1 + C_4.l_2^2/l_1 + C_5.l_2^2/l_1 + C_6.l_2^2/l_1,$
$C_{5,6} = C_{6,5} = C_{c1}.e_2 - C_{c2}.e_2 + C_{c3}.e_2 - C_{c4}.e_2 + C_1.a_1 - C_2.a_1 + C_3.l_2^2/l_1.a_1 - C_4.l_2^2/l_1.a_1 + C_5.l_2^2/l_1.a_1 - C_6.l_2^2/l_1.a_1;$
$C_{5,7} = C_{7,5} = -C_{c1}.b_4 - C_{c2}.b_4 - C_{c3}.b_5 - C_1.b_1 - C_2.b_1 + C_3.l_2^2/l_1.b_2 + C_4.l_2^2/l_1.b_2;$
$C_{5,8} = C_{8,5} = -C_1 - C_2,$
$C_{5,9} = C_{9,5} = C_{6,8} = C_{8,6} = -C_1.a_1 + C_2.a_1,$
$C_{5,10} = C_{10,5} = -C_3.l_2^2/l_1 - C_4.l_2^2/l_1;$

$C_{5,11} = C_{11,5} = C_{6,10} = C_{10,6} = -C_3.l_2^2/l_1.a_1 + C_4.l_2^2/l_1.a_1$
$C_{5,12} = C_{12,5} = C_{6,12} = C_{12,6} = -C_5.l_2^2/l_1 + C_6.l_2^2/l_1;$

$C_{5,13} = C_{13,5} = -C_5.l_2^2/l_1.a_1 + C_6.l_2^2/l_1.a_1,$
$C_{6,6} = C_{c1}.e_2^2 + C_{c2}.e_2^2 + C_{c3}.e_2^2 + C_{c4}.e_2^2 + C_1.a_1^2 + C_2.a_1^2 + C_3.l_2^2/l_1.a_1^2 + C_4.l_2^2/l_1.a_1^2 + C_5.l_2^2/l_1.a_1^2 + C_6.l_2^2/l_1.a_1^2;$
$C_{6,7} = C_{7,6} = -C_{c1}.b_4.e_2 + C_{c2}.b_4.e_2 - C_{c3}.b_5.e_2 + C_{c4}.b_5.e_2 - C_1.a_1.b_1 + C_2.a_1.b_1 + C_3.l_2^2/l_1.b_2.a_1 - C_4.l_2^2/l_1.b_2.a_1 + C_5.l_2^2/l_1.a_1 - C_6.l_2^2/l_1.a_1;$

$C_{6,9} = C_{9,6} = -C_1.a_1^2 - C_2.a_1^2,$
$C_{6,11} = C_{11,6} = -C_3.l_2^2/l_1.a_1^2 - C_4.l_2^2/l_1.a_1^2,$
$C_{6,13} = C_{13,6} = -C_5.l_2^2/l_1.a_1^2 - C_6.l_2^2/l_1.a_1^2,$

$C_{7,7} = C_{c1}.b_4^2 + C_{c2}.b_4^2 + C_{c3}.b_5^2 + C_{c4}.b_5^2 + C_1.b_1^2 + C_2.b_1^2 + C_3.l_2^2/l_1.b_2^2 + C_4.l_2^2/l_1.b_2^2 + C_5.l_2^2/l_1.b_3^2 + C_6.l_2^2/l_1.b_3^2;$

$C_{7,8} = C_{8,7} = C_1.b_1 + C_2.b_1,$
$C_{7,9} = C_{9,7} = C_1.a_1.b_1 - C_2.a_1.b_1,$
$C_{7,10} = C_{10,7} = -C_3.l_2^2/l_1.b_2 - C_4.l_2^2/l_1.b_2,$

$C_{7,11} = C_{11,7} = -C_3.l_2^2/l_1.b_2.a_1 + C_4.l_2^2/l_1.b_2.a_1,$
$C_{7,12} = C_{12,7} = -C_5.l_2^2/l_1.b_3 - C_6.l_2^2/l_1.b_3,$

$C_{7,13} = C_{13,7} = -C_5.l_2^2/l_1.b_3.a_1 + C_6.l_2^2/l_1.b_3.a_1,$
$C_{8,8} = C_1 + C_2, C_{8,9} = C_{9,8} = C_1.a_1 - C_2.a_1;$

$C_{9,9} = C_{9,8} = C_1.a_1^2 + C_2.a_1^2,$
$C_{10,10} = C_3.l_2^2/l_1 + C_4.l_2^2/l_1, C_{10,11} = C_{11,10} = C_3.l_2^2/l_1.a_1 - C_4.l_2^2/l_1.a_1;$
$C_{11,11} = C_3.l_2^2/l_1.a_1^2 + C_4.l_2^2/l_1.a_1^2,$
$C_{12,12} = C_5.l_2^2/l_1 + C_6.l_2^2/l_1,$
$C_{12,13} = C_{13,12} = C_5.l_2^2/l_1.a_1 - C_6.l_2^2/l_1.a_1$

$C_{13,13} = C_5.l_2^2/l_1.a_1^2 + C_6.l_2^2/l_1.a_1^2;$

$K_{1,1} = K_s,\ K_{1,2} = -K_s,\ K_{1,3} = K_s.e_1,\ K_{1,4} = K_s.d_1;$

$K_{2,1} = -K_s, K_{2,2} = 4K_c + K_s, K_{2,3} = -K_s.e_1,$
$K_{2,4} = K_c(2d_3 - 2d_2) - K_s.d_1, K_{2,5} = -4K_c, ,$
$K_{2,7} = K_c(2b_5 + 2b_4);$

$K_{3,1} = K_s.e_1,\ K_{3,2} = -K_s.e_1,$
$K_{3,3} = 4K_c.e_2^2 + K_s.e_1^2,\ K_{3,4} = K_s.e_1.d_1;$

$K_{4,1} = K_s.d_1, K_{4,2} = -K_s.d_1 - 2K_c.d_2 + 2K_{c3}.d_3,$
$K_{4,3} = K_s.d_1.e_1, K_{4,4} = K_s.d_1^2 + 2K_c(d_2^2 + d_3^2),$
$K_{4,5} = 2K_c(d_2 - d_3), K_{4,6} = -2K_c.d_3.e_2,$
$K_{4,7} = -2K_c.d_2.b_4 + 2K_c.d_3.b_5;$

$K_{5,2} = -4K_c, K_{5,4} = -2K_c.d_3$
$K_{5,5} = 2K_f + 2K_m + 2K_r + 4K_c,$
$K_{5,6} = 2(K_f + K_m + K_r).a_1 + 2K_c.e_2,$
$K_{5,7} = -2K_f.b_1 + 2K_m.b_2 + 2K_r.b_3 - 2K_c.b_4,$
$K_{5,8} = -2K_f, , K_{5,10} = -2K_m, K_{5,11} = 2K_m.a_1$
$K_{5,12} = -2K_r;$

$K_{6,2} = -2K_c.e_2,\ K_{6,3} = -2K_c.e_2^2,$
$K_{6,4} = -2K_c.e_2.d_3,$
$K_{6,5} = 2(K_f + K_m + K_r).a_1 + 2K_c.e_2,$
$K_{6,6} = 2(K_f + K_m + K_r).a_1^2 + 4K_c.e_2^2,$
$K_{6,7} = -2K_f.a_1.b_1 - 2K_m.a_1.b_2 + 2K_r.a_1.b_3 - 2K_c.e_2.b_4$
$, K_{6,8} = -2K_f.a_1, , K_{6,12} = -2K_r.a_1;$

$K_{7,2} = 4K_c.b_4, K_{7,4} = -2K_c.b_4.d_2 + 2K_c.b_5.d_3,$
$K_{7,5} = -2K_f.b_1 + 2K_m.b_2 + 2K_r.b_2 - 2K_c.b_4 - 2K_c.b_5$
$K_{7,6} = -2K_f.a_1.b_1 + 2K_5.a_1.b_3 + 2K_c.e_2.b_4,$
$K_{7,7} = 2K_f.b_1^2 + 2K_m.b_2^2 + 2K_r.b_3^2 + 2K_c.b_4^2 + 3K_c.b_5^2$
$, K_{7,8} = 2K_f.b_1, K_{7,10} = -2K_m.b_2,$
$K_{7,11} = 2K_m.b_2.a_1, K_{7,12} = -2K_r.b_3;$

$K_{8,6} = -2K_f.a_1, K_{8,7} = 2K_f.b_1, K_{8,8} = 2K_f + 2K_{wf};$

$K_{9,9} = 2K_{wf}.a_2{}^2 + 2K_1.a_1{}^2\, K_{9,14} = -K_{wf}.a_2,$
$K_{9,15} = K_{wf}.a_2;$

$K_{10,5} = -2K_m, K_{10,6} = -2K_m.a_1, K_{10,7} = -2K_3.b_2.,$
$K_{10,10} = 2K_{wr}, K_{10,11} = -2K_3.a_1, K_{10,16} = -K_{wr},$
$K_{10,17} = -K_{wr};$

$K_{11,5} = 2K_m.a_1, K_{11,7} = 2K_m.b_2.a_1,$
$K_{11,10} = -2K_m.a_1, K_{11,11} = 2K_m.a_1{}^2 + 2K_{wr}.a_2{}^2,$
$K_{11,16} = -K_{wr}.a_2, K_{11,17} = K_{wr}.a_2;$

$K_{12,5} = -2K_r, K_{12,6} = -2K_5.a_1, K_{12,7} = -2K_r.b_3,$
$K_{12,12} = 2K_{wr}, , K_{12,18} = -2K_{wr};$

$K_{13,13} = 2K_{wr}.a_2{}^2 + 2K_5.a_1{}^2, K_{13,18} = -K_{wr}.a_2,$
$K_{13,19} = -K_{wr}.a_2;$

$K_{14,8} = -K_{wf}, K_{14,9} = -K_{wf}.a_2, K_{14,14} = K_{wf};$

$K_{15,8} = -K_{wf}, K_{15,9} = K_{wf}.a_2, K_{15,15} = K_{wf};$

$K_{16,10} = -K_{wr}, K_{16,11} = -K_{wr}.a_2, K_{16,16} = K_{wr};$

$K_{17,10} = -K_{wr}, K_{17,11} = K_{wr}.a_2, K_{17,17} = K_{wr};$

$K_{18,12} = -K_{wr}, K_{18,13} = K_{wr}.a_2, K_{18,18} = K_{wr};$

$K_{19,12} = -K_{wr}, K_{19,13} = -K_{wr}a_2, K_{19,19} = K_{wr};$

In which, C_s and K_s are the damping coefficient and stiffness of spring of driver seat; C_c and K_c are the damping and stiffness of each spring of cab suspension; C_1,C_2 are front suspension damping; $C_{3\sim6}$ are the drive suspension coefficient; C_e is the effective damping coefficient of drive axle suspension; K_f is the stiffness of each spring of front axle suspension; K_m, and K_r are defined for stiffness of every spring for the middle axle and the rear axle, respectively; K_{wf} is also considered for the equivalent stiffness of each of front tires, while K_{wr} plays the same role for the tires of middle and rear wheels. Other variables and constants were illustrated in the previous sections.

The developed dynamic model is 19 DoF, which includes the truck and its 6 wheels. However, in trucks motion analysis under sinusoidal road surface excitation, because of that the truck is placed on the road and the effect of the excitations of the road surface on the motions of the 6 wheels, therefore a 13 DoF system have been used as a simplified model of the 19 DoF model stiffness matrix and the proper model.

The following sinusoid inputs is the excitations profile of the road surface that applies to the wheels:

$w_i = A_r \sin(\omega_{dr} t + \phi_i);$
$1,2,\dots,6$
(6)

$$\omega_{dr} = 2\pi\left(\frac{v}{L}\right); \qquad (7)$$

Where A_r is road roughness magnitude in meter, ω_{dr} is drive frequency in rad/s, v is truck forward speed in m/s, L is Road surface wave length in meter and ϕ_i is the phase angle of the nth wheel in rad.

And the equation of motion is as below:

$$M.\ddot{W} + C.\dot{W} + K.W = f(t); \qquad (8)$$

Where $\mathbf{M}$ is system mass matrix, $\mathbf{C}$ is damping matrix, $\mathbf{K}$ is stiffness matrix, $\ddot{W}$ is acceleration vector, $\dot{W}$ is velocity vector, W is displacement vector, all of the 13 DoF truck model and $f(t)$ is road excitation vector, which is defined in the form of:

$$f(t) = \begin{bmatrix} 0 \\ \vdots \\ 0 \\ k_{w1}A_r\sin(\omega_{dr}t+\phi_1) + k_{w2}A_r\sin(\omega_{dr}t+\phi_2) \\ k_{w1}a_2A_r\sin(\omega_{dr}t+\phi_1) - k_{w2}a_2A_r\sin(\omega_{dr}t+\phi_2) \\ k_{w3}A_r\sin(\omega_{dr}t+\phi_3) + k_{w4}A_r\sin(\omega_{dr}t+\phi_4) \\ k_{w3}a_2A_r\sin(\omega_{dr}t+\phi_3) - k_{w4}a_2A_r\sin(\omega_{dr}t+\phi_4) \\ k_{w5}A_r\sin(\omega_{dr}t+\phi_5) + k_{w6}A_r\sin(\omega_{dr}t+\phi_6) \\ k_{w5}a_2A_r\sin(\omega_{dr}t+\phi_5) - k_{w6}a_2A_r\sin(\omega_{dr}t+\phi_6) \end{bmatrix}_{(13\times1)}$$

As mentioned system matrices in Equation (8) is 13×13, the vector G (gravity vector) does not appear here, because the systems initial positions are chosen to be in the equilibrium positions.

Central difference method has been utilized for numerical solution and dynamic simulation, the well-known equation for it is as below:

$$\ddot{w} \approx \frac{W_{t+\Delta t} - 2w_t + w_{t-\Delta t}}{(\Delta t)^2}; \qquad (9)$$

$$\dot{w} \approx \frac{w_{t+\Delta t} - w_{t-\Delta t}}{2\Delta t}; \qquad (10)$$

The continuous sinusoidal variation of the road profile, which is used in the simulation, is as below:

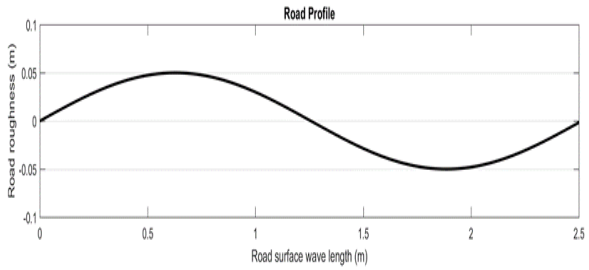

Fugure 5. Road profile

In this paper, for simulating typical road conditions, two drive frequencies have been used. The low drive frequency is chosen to have a magnitude of 2 Hz and the higher drive frequency have a magnitude of 12 Hz. The difference between the road roughness excitations caused by these two drive frequencies is showed in figure below:

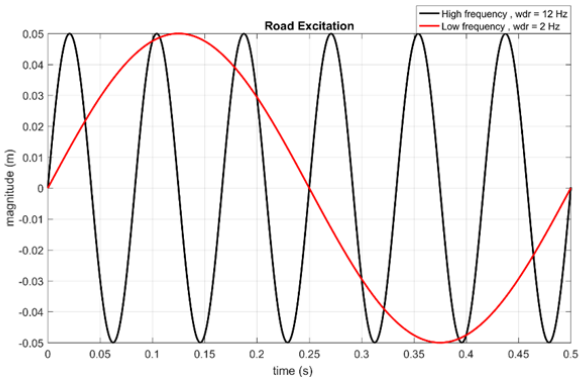

Figure 6. The high and low frequency for road excitations cases.

Two cases have been chosen for phase angle (ϕ). In one case the right steer wheel and the left steer wheel have no phase difference, and this means that ϕ12 is equal to 0 and in the other case we have considered 90 degrees' phase lag for the right steer wheel compared to the left steer wheel and this similarly means that ϕ12 is equal to π/2. For comparison, these two cases with various phase angles are showed in Figure 7.

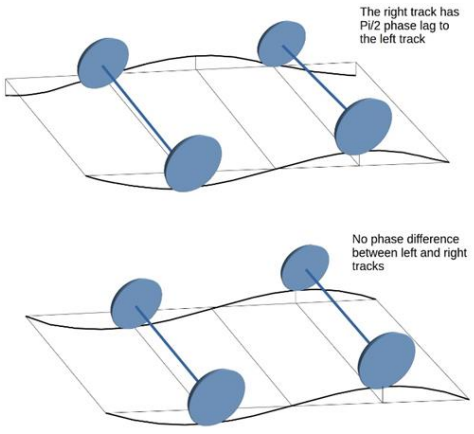

Figure 7. various excitation phase angles between the right and the left wheel.

By considering the depicted phase angles, the nth wheel's phase angle (ϕn) is evaluated as follow:

$$\phi_1 = 0;$$

$$\phi_2 = \phi_1 - \phi_{12};\ \phi_3 = \phi_1 - \phi_{13};\ \phi_4 = \phi_2 - \phi_{24};$$

$$\phi_5 = \phi_1 - \phi_{15};\ \phi_6 = \phi_2 - \phi_{26};$$

Where ϕ12, ϕ13, … are wheel 1 and 2, wheel 1 and 3, etc. phase angle difference as following:

ϕ_12=0 or π/2 ; (depends on case of study);

$$\phi_{13} = \frac{2\pi(b_1 - b_2)}{L};$$

$$\phi_{15} = \frac{2\pi(b_1 - b_3)}{L};\ \phi_{24} = \phi_{13};\ \phi_{26} = \phi_{15};$$

L is the wave length of road surface in meter and b1, b2, b3 are some geometric distance, depicted in figure 4.

The drive frequency for the truck can be specified in two ways. In one way by assuming a specific road with a fixed wave length of L, a higher drive frequency means that the truck is running in a higher speed, while in a lower drive frequency the truck is running at a lower speed. Analogously for the other way, if we consider a fixed truck speed, a higher drive frequency means that the road surface has short wavelength characteristics, while in a lower drive frequency the road surface has long wavelength characteristics. Therefore, the assumptions in the simulation strongly affects the simulation results. In this paper, the wave length of the road is considered to be fixed and the truck speed is set to either the high and low values of 30m/s and 5m/s, respectively. By considering two different ϕn settings this gives us four cases in total, for case 1 and 2 we have a high drive frequency and for case 3 and 4 we have low dive frequency, for all cases ωdr is 2Hz and Ar is 0.05m, for case 1 and 3, ϕ12 is equal to zero and for case 2 and 4, ϕ12 is equal to π/2. Finally, by programming the equations in MATLAB software, the simulation results are achieved.

3. RESULTS

The results for the four expressed cases are shown by the following figures as system time response for the different cases.

Case 1:

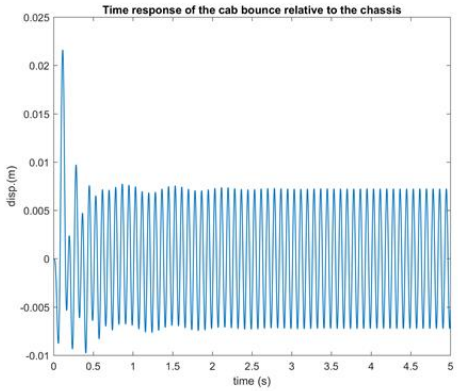

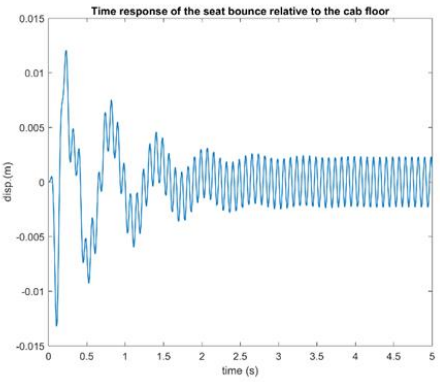

Figure 8. Cab to chassis and seat to cab floor relative bounce time response in high drive frequency for $\phi 12 = 0$

Case 2:

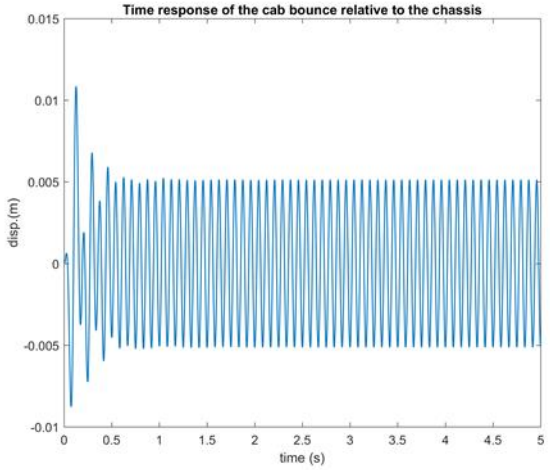

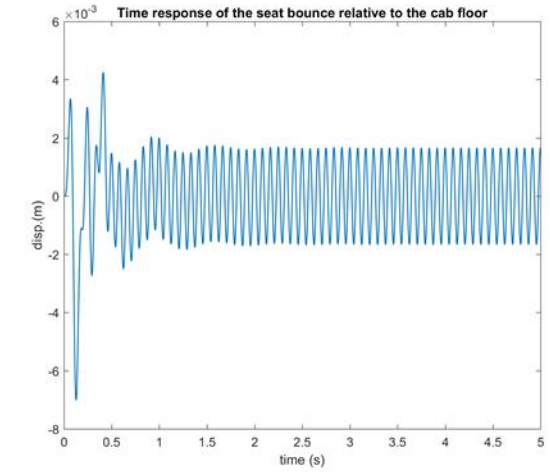

Figure 9. Cab to chassis and seat to cab floor relative bounce time response in high drive frequency for $\phi 12 = \pi/2$.

Case 3:

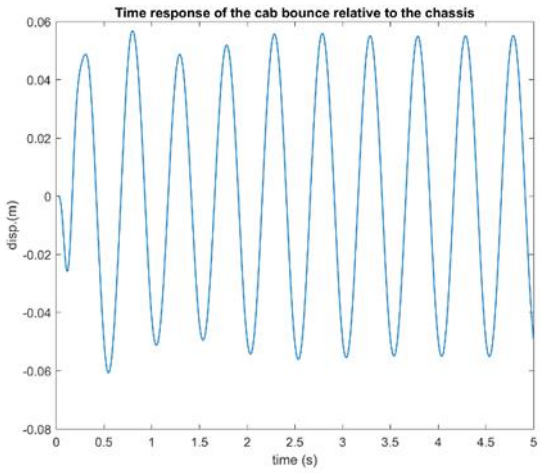

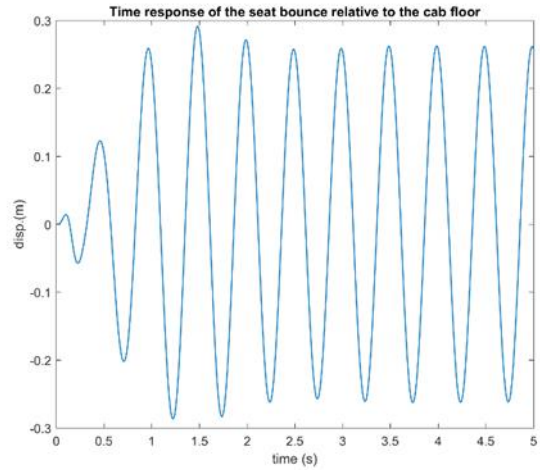

Figure 10. Cab to chassis and seat to cab floor relative bounce time response in low drive frequency for $\phi 12 = 0$

Case 4:

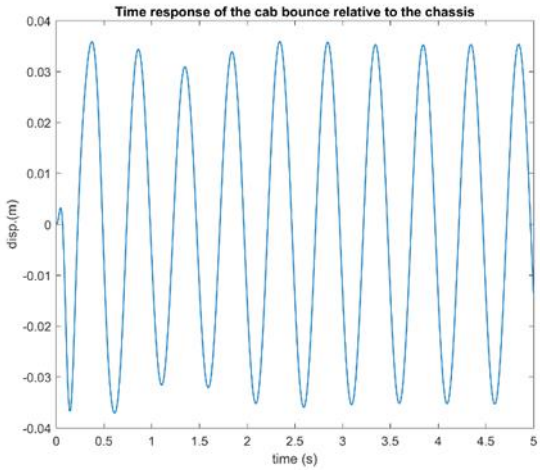

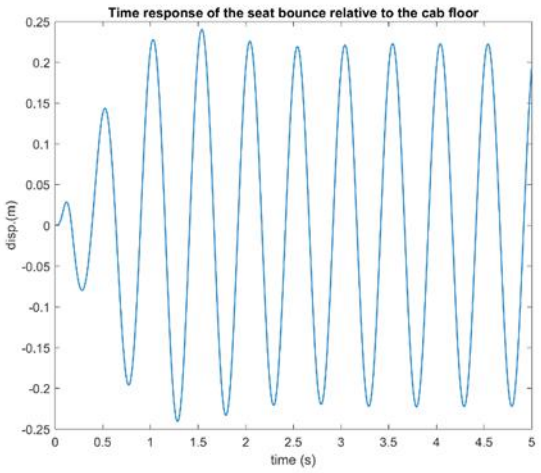

Figure 11. Cab to chassis and seat to cab floor relative bounce time response in low drive frequency for $\phi 12 = \pi/2$

These cases from Figure 8 to Figure 11 shows the bounces of the seat and the cab relative to the cab floor and the chassis, respectively as it is more conventional to measure in this way. Results illustrates that the seat has an acceptable vibration isolation performance in high frequency excitations. However, in relatively lower frequency excitations, it is clear that the vibration level is extremely high and is greatly magnified.

4. CONCLUSION

The three-axle truck in this work have been modeled as a 19-DoF system. The linear model of the truck has some unique features which includes the cab suspension, the seat suspension and the suspension geometry, this features are vital in ride modeling for heavy vehicles but are often ignored. The physical properties of the truck are evaluated by modelling the truck in SOLIDWORKS software. The equations of motion are obtained by using the Lagrange equation. To obtain the system responses subject to sinusoidal road excitations numerical central difference method is assisted. Finally, system's time responses have been gained under four cases for the truck in low and high speed motions, these are useful to know the vibrating component of the truck. Although, some of these results may only affect this special truck model, they will help to better understand the traits of this kind of vehicles and also will help to understand how to develop more realistic nonlinear models.

5. REFERENCES

[1] Ali Rahmani, Ali Mirmohammadi, S. M. Javad Zeidi, Saeed Shojaei, "Numerical Approach toward Calculation of vibration Characteristics of the Multi Axles Truck Using Lagrange Method".

[2] Saeed Shojaei, S. M. Javad Zeidi, Ali Rahmani, Ali Mirmohammadi, "Analytical Analysis Approach to Study of the Vibration Characteristics of the Multi Axles Truck and its Validation".

[3] Hamedi, A., Ketabdar, M. (2016). Energy Loss Estimation and Flow Simulation in the skimming flow Regime of Stepped Spillways with Inclined Steps and End Sill: A Numerical Model. International Journal of Science and Engineering Applications, 5(7), 399-407.

[4] Kadkhodapour, J. and S. Raeisi, Micro–macro investigation of deformation and failure in closed-cell aluminum foams. Computational Materials Science, 2014. 83: p. 137-148.

[5] Ketabdar, M. Hamedi, A. (2016). Intake Angle Optimization in 90-degree Converged Bends in the Presence of Floating Wooden Debris: Experimental Development. Florida Civil Engineering Journal, 2, 22-27.

[6] Sheikholeslami ,A. and L. Azizi, (2010). Safety Analysis of Constructed U-turns in the City of Tehran], Journal of Transportation Research 7 (223), 167-184.

[7] Azizi, L. and A. Sheikholeslami, (2013). Safety effect of U-turn Conversions in Tehran: Empirical Bayes Observational Before and After Study and Crash Prediction Models", Journal of Transportation Engineering 139 (1),101-108.

[8] Kadkhodapour, J., H. Montazerian, and S. Raeisi, Investigating internal architecture effect in plastic deformation and failure for TPMS-based scaffolds using simulation methods and experimental procedure. Materials Science and Engineering: C, 2014. 43: p. 587-597.

[9] Sheikholeslami, A and L. Azizi, (2010) Observational Before-After Study of the Safety Effect of U-turns Conversions Using the Empirical Bayes Method, 15th International Conference on Road Safety CMRSC-XX

[10] Mardanpour, P., Izadpanahi, E., Rastkar, S., Fazelzadeh, S. A., & Hodges, D. H. (2017). Geometrically Exact, Fully Intrinsic Analysis of Pre-Twisted Beams Under Distributed Follower Forces. AIAA Journal, 1-13.

[11] Mardanpour, P., Izadpanahi, E., Rastkar, S., & Hodges, D. H. (2017). Nonlinear Aeroelastic Gust Suppression and Engine Placement. Journal of Aircraft, 1-4.

[12] Mardanpour, P., Izadpanahi, E., Rastkar, S., & Hodges, D. H. (2017). Effects of engine placement on nonlinear aeroelastic gust response of high-aspect-ratio wings. In AIAA Modeling and Simulation Technologies Conference (p. 0576).

[13] Watts GR (1987) Traffic-induced ground-borne vibrations in dwellings. Research Report 102, Transport and Road Research Laboratory, Crowthorne, Berkshire

[14] Hunt HEM (1991) Modelling of road vehicles for calculation of traffic-induced ground vibrations as a random process. J Sound Vib 144(1):41–51. doi:10.1016/0022-460X(91)90731-X

[15] Cebon D (1993) Interaction between heavy vehicles and roads. Warrendale (USA): Society of Automotive Engineers, SP 951: ISBN: 1-56091-336-3

[16] Mamlouk MS (1997) General outlook of pavement and vehicle dynamics. J Transport Eng 123(6): 515-517. ISSN: 0733-947X

[17] Liu C, Herman R (1998) Road profiles, vehicle dynamics, and human judgement of serviceability of roads: spectral frequency domain analysis. J Transport Eng 124(2):106–111. doi:10.1061/(ASCE)0733-947X(1998)124:2(106)

[18] Melcer J (2006) Vehicle-road interaction, analysis in a frequency domain. Slovak J Civil Eng 3: 48–52. ISSN: 1210-3896

[19] Dodds CJ, Robson JD (1973) The description of road surface roughness. J Sound Vib 31(2):175–183. doi:10.1016/S0022-460X(73)80373-6

[20] Rahmani, F., Razaghian, F. and Kashaninia, A.R., 2015. Novel Approach to Design of a Class-EJ Power Amplifier Using High Power Technology. World Academy of Science, Engineering and Technology, International Journal of Electrical, Computer, Energetic, Electronic and Communication Engineering, 9(6), pp.541-546.

[21] Wambold JC, Defrain LE, Hegmon RR, Macghee K, Reichert J, Spangler EB (1981) State of the art of measurement and analysis of road roughness. Transport Res Rec 836: 21–29. ISSN: 0361-1981

[22] ISO 8608 (1995) Mechanical vibration, road surface profiles. Reporting of Measured Data

[23] Andren P (2006) Power spectral density approximations of longitudinal road profiles. Int J Veh Des 40(1/2/3):2–14. doi:10.1504/IJVD.2006.008450

[24] Elson MJ, Bennet JM (1995) Calculation of the power spectral density from surface profile data. Appl Opt 34:201–208. doi:10.1364/AO.34.000201

[25] Feng T, Yu-Fen H, Shun-Hsu T, Wes SJ (2006) Generation of random road profiles. CSME: B04-001: 1373-1377

[26] Azizi, L., MS. Iqbal and M.Hadi,(2018), Estimation of Freeway Platooning Measures Using Surrogate Measures Based on Connected Vehicle Data, Presented at 97st Annual Meeting of Transportation Research Board, Washington DC.

[27] Wong. J, Y.," Theory of ground vehicles". John Wiley & Sons, Canada. (2001)

[28] Rahmani, F., Razaghian, F. and Kashaninia, A.A., 2014. High Power Two-Stage Class-AB/J Power Amplifier with High Gain and Efficiency. Journal of Academic and Applied Studies (JAAS), 4(6), pp.56-68.

[29] Jazar, R., "Advanced Vibrations:A modern Approach", Springer, New York. (2013).

[30] Jazar, R., "Vehicle Dynamics: Theory and Application", Springer, New York. (2010).

[31] Gillespie, T, D., "Fundamentals of Vehicle Dynamics", SAE publishing group, United States of America. (1992).

[32] Yang, X., Zengcai, W., Weili, P., "Coordinated Control of AFS and DYC for Vehicle Handling and Stability Based on Optimal Guaranteed Cost Theory," Vehicle System Dynamics, 47, pp. 57-79 (2009).

[33] Zheng, S., Tang, H., Han, Z., Zhang, Y., "Controller Design for Vehicle Stability Enhancement," Control Engineering Practice, 14, pp. 1413-1421 (2006).

[34] A. Rahmani-Hanzaki, S. K. Saha, and P. V. M. Rao, An improved recursive dynamic modeling of a multibody system with spherical joint, Int, J, of Multibody system dynamics, 21, pp. 325-345, (2009).

[35] Tabatabaee, S,H,. "Integrated control to improve directional stability and maneuverability of the articulated heavy vehicle", PhD Thesis, K. N. Toosi University of Technology Faculty of Mechanical Engineering, (2013).

[36] Zeidi, SMJ, Hoseini, P., Rahmani, A., (2017). Study of vibration specifications of a three-axle truck using Lagrange method, Journal of Modern Processes in Manufacturing and Production, vol. 6(1), pp. 83-95.

[37] Zeidi, SMJ, Hoseini, P., Rahmani, A., (2017). Modeling a Three-axle Truck and Vibration Analysis under Sinusoidal Road Surface Excitation, International Journal of Science and Engineering Applications Volume 6 Issue 09, 2017.

[38] Zeidi, SMJ and Mahdi, M. 2015. Investigation effects of injection pressure and compressibility and nozzle entry in Diesel injector nozzle's flow. Journal of Applied and Computational Mechanics. 1(2):83–94.

[39] Zeidi, SMJ., and Mahdi, M. 2015. Effects of nozzle geometry and fuel characteristics on cavitation phenomena in injection nozzles. Proceedings of the 22st Annual International Conference on Mechanical Engineering-ISME.

[40] Zeidi, SMJ. and Mahdi. M. 2014. Investigation of viscosity effect on velocity profile and cavitation formation in Diesel injector nozzle. Proceedings of the 8th International Conference on Internal Combustion Engines.

[41] Zeidi, SMJ. and Mahdi, M. 2015. Evaluation of the physical forces exerted on a spherical bubble inside the nozzle in a cavitating flow with an Eulerian/Lagrangian approach, European Journal of Physics, 36(6):41-65.

[42] SM Aghaei, MM Monshi, I Torres, SMJ Zeidi, I Calizo, 2018, DFT study of adsorption behavior of NO, CO, NO2, and NH3 molecules on graphene-like BC3: A search for highly sensitive molecular sensor, Journal of Applied Surface Science, 427, PP. 326-333.

International Journal of Science and Engineering Applications
Volume 7–Issue 06,94-100, 2018, ISSN:-2319–7560

Design Model of Horizontal Axis Wind Turbine Blade at Technological University (Thanlyin)

Hti Lar Tun Kyi
Department of Mechanical Engineering,
Technological University
Thanlyin, Myanmar

Theingi
Department of Mechanical Engineering,
Technological University
Thanlyin, Myanmar

Khaing Thida
Department of Mechanical Engineering,
Technological University
Thanlyin, Myanmar

Abstract: In this study, a horizontal axis wind turbine (HAWT) blade with 1 kW power output has been designed for Technological University (Thanlyin) and the blade aerodynamics are also simulated to investigate its flow structures and aerodynamic characteristics. As the technology of wind power generation is improved; the blade of wind turbine is becoming the main sector for perfect and effective design. The designed wind turbine blade should have enough strength, stiffness, elasticity, hardness and stability. Therefore, modeling and strength check of wind turbine blade is very important for the designing of wind turbines. This paper purposes to express the design calculation and strength check of HAWT blade. In this paper, the selection of airfoil shape from NACA series was done by using Comsol Multiphysics software and the 3D model of blade was proactive by using Design Foil and SolidWorks software. Finite element analysis on the blade was done in SolidWorks. The numerical simulation for strength check was done by investigating the Von Mises Stress distribution over the blade.

Keywords: modeling; strength; airfoil; aerodynamic; blade element theory; finite element analysis

1. INTRODUCTION

There are varieties of clean energy sources available on the world. The sustainable resources such as sun, water and wind are very important and significant renewable sources of nature. Many of scientists and technologists are trying to produce the clean and effective energy from natural sources. Among renewable energy sources for Myanmar, wind is the most widely used resource due to its commercial acceptance, low cost and ease of operation and maintenance, and least adverse effect on the environment.

Wind power is really cost effective and also a free, clean and inexhaustible energy source. It is a proven, reliable and practically extractable source of energy for desired power generation. It is also a fast growing form of alternative energy has a potential to make an impact and community. Over hundreds of years, power has been extracted from the wind with many historic designs. The improved understanding of aerodynamics and advances in materials, has led to the return of wind energy extraction in the latter half of the 20th century.

Wind energy is an abundant resource in comparison with other renewable resources. Wind power devices are now used to produce electricity, and commonly termed wind turbines. A wind turbine is a device that converts the wind`s kinetic energy to electrical energy. A variety of wind turbines are being designed, manufactured and fabricated. A turbine with a shaft mounted horizontally parallel to the ground is known as a horizontal axis wind turbine (HAWT). A vertical axis wind turbine (VAWT) has its shaft normal to the ground.

A conventional horizontal axis wind turbine (HAWT) can be divided into three main components;
(i)rotor component includes the blades and hub for converting wind energy to low speed rotational energy,
(ii)generator component includes electrical generator, control electronics, gear box and variable transmission component for converting low speed to high speed rotation,
(iii)structural support component includes the tower and yaw mechanism [1].

2. DESIGN CALCULATION OF BLADE

2.1 Site Location

Technological University (Thanlyin)
Yangon Division, Myanmar
Reference height, z_{ref} = 50m
Wind velocity at 50m, v_{zr} = 4.6m/s
Tower height, h = 10.668m (above the ground)
The elevation of tower above sea level, z = 31.6992m

This location has the annual temperature of 92° F. The density (ρ_{air}) and dynamic viscosity (μ) of air are 1.2214kg/m^3 and 1.788x10^{-5} N-s/ m^2 respectively. It is near the sea and also the suburbs area of Thanlyin. So, the value of terrain index (m) is 0.257 [2].

Annual average wind speed at z,

$$v_{average} = v_z = v_{zr} (z / z_{ref})^m = 4.092 \text{m/s} \quad (1)$$

It is needed to calculate the design wind speeds of Site Location. The relation of annual average wind speed and design wind speeds are shown in Table 1.

Table 1. Relations and results of wind speed

Types of Wind Speed	Relations with Average Wind Speed	Results (m/s)
$v_{average}$		4.092
v_{cut-in}	0.7 $v_{average}$	2.864
v_{rated}	2 $v_{average}$	8.184
$v_{cut-out}$	3 $v_{average}$	12.276

2.2 Sizing Rotor

$$\eta_{overall} = C_p \, \eta_{mechanical} \, \eta_{generator} \quad (2)$$

Max. power coefficient, C_p= 0.8 Betz`s limit = 0.4741

For wind turbine, $\eta_{mechanical}$ = 96%

Generator efficiency in general, $\eta_{generator}$ = 70%

∴ System overall efficiency, $\eta_{overall}$ = 0.3186

Power = $0.5\rho_{air} A v_{rated}^3 \eta_{overall}$ (3)

Rotor swept area, $A = 9.3763 m^2$

∴ Blade length, R = 1.7276m

Solidity, $\sigma = Bc/(2\pi R)$ (4)

For three blade rotor (B=3), solidity should be taken between 4.5% and 5%.

For σ = 4.9%, chord length, c = 0.1773m

2.3 Optimization of Airfoil

Blade optimization is the main sector for resulting higher efficiency of wind turbine. The optimized airfoil design can contrive the optimized blade design model and also give out the higher efficiency of wind turbine. So, airfoil optimization is very essential and important for the design of wind turbine blade and also the structure of wind turbine.

Comsol Multiphysics is commercial software that can solve many problems from Science and Mathematics fields. Selection of airfoil depends on the maximum value of lift/drag ratio and maximum lift force for better performance of wind turbine. Domain size is needed to be enough for calculating of flow field around airfoil. Initially, the Software defined the domain size as build in. The selection of enough domain size may cause no boundary effect.

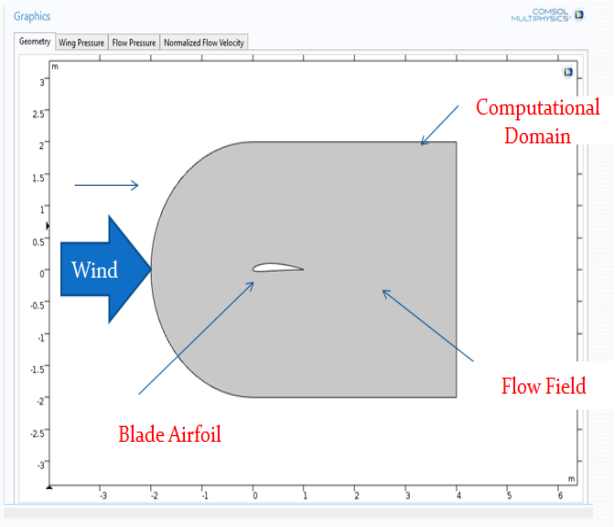

Figure 1. The CFD analysis in Comsol Multiphysics

The flow can be classified as Laminar and Turbulent according to Reynolds Number. If the flow was laminar, the mesh will be made coarsely. If the flow was turbulent, we can find the flow field stress and velocity by using Sparlet-Allmaras Turbulent Model.

Reynolds Number, $Re = \rho_{air} v_{average} c/\mu$ (5)

= 49560 (Approximated)

By using Comsol Multiphysics software, the airfoil can be chosen at Re = 49560. Firstly, it is necessary to choose most common airfoil shapes for three bladed wind turbines. Then, the airfoil which can give maximum ratio of lift coefficient (C_L) and drag coefficient (C_D) to make the design efficient must be selected.

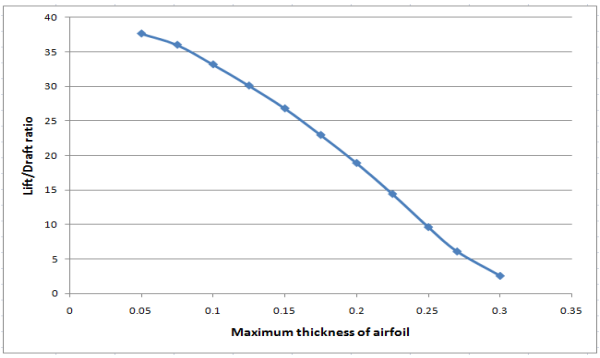

Figure 2. Lift/drag ratio Vs maximum thickness of airfoil

According to the Figure 2, the curve is conspicuously clear. It is seen that the lift/drag ratio and maximum thickness of airfoil are inversely proportional. The increasing of airfoil thickness can cause the decreasing of lift/drag ratio. So, in the design of wind turbine blade, the minimum value of airfoil thickness will gain the optimum condition.

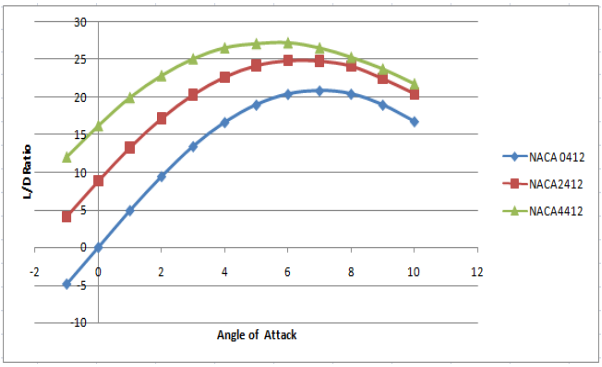

Figure 3. Lift/ drag ratio respect to angle of attack

According to the Figure 3, NACA- 4412 was chosen in order to get the maximum ratio of (C_L) and (C_D).

C_L/C_D is maximum at angle of attack $\alpha = 6^o$.

C_L=1.034, C_D=0.03792 and C_L/C_D = 27.2679

2.4 Design Parameters of Each Section

To make modeling, the designed parameters are to be calculated and so the detailed shape of geometry of the blade profile will be available for strength check. The blade chord length for each section will vary with the radius of the blade. The twist angle (or blade setting angle) has to be determined. The areas of sections must be calculated to investigate the surface aerodynamic load on the blade surface.

The angle of attack depends on the linear speed of each local radius. The twisted blade is more efficient than constant blade due to the optimum angle of attack for each radius. The blade is divided into (10) equal sections.

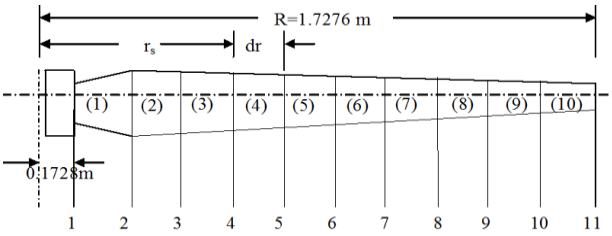

Figure 4. Elements of blade section

The length 0.1728m at the root of blade is to attach the blade and hub. The numbers 1 to 10 within parentheses are referring to the 10 elements and the numbers 1 to 11 are blade sections number from root to tip of the blade. Radius of rotor axis to each section are denoted by r_s , the subscript (s) refers to the section number.

$dr = (1.7276-0.1728)/10 = 0.1555$ m

$r_1 = 0.1728$ and $r_s = r_{s-1}+dr$ (6)

Speed ratio at each section, $\lambda_r = \lambda \times r_s/R$ (7)

Tip speed ratio, $\lambda = 6$ for three blade rotor

By substituting r_1 to r_{11} values in Equation (7), speed ratio at each radius can be calculated and their respective shape parameters can be defined [3]. So, speed ratio of each radius is 0.60, 1.14, 1.68, 2.22, 2.73, 3.30, 3.84, 4.38, 4.92, 5.46, 6.00 and shape parameters are 3.20, 3.15, 1.60, 1.17, 0.70, 0.55, 0.40, 0.32, 0.25, 0.19, 0.17respectively.

2.5 Dimensions of Airfoil

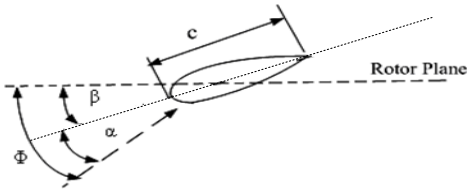

Figure 5. Blade angles and chord length of airfoil

Chord length, $c = (r_s \times SP)/(C_L \times B)$ (8)

Twist angle, $\phi = \tan^{-1}(2/3\lambda_r)$ (9)

Blade setting angle, $\beta = \phi - \alpha$ (10)

Airfoil maximum thickness, $t = 0.12xc$ (11)

For each section, chord length, twist angle, blade setting angle and airfoil maximum thickness can be calculated and these results are shown in Table 2. [4].

Table 2. Lift and drag ratio respect to angle of attack

Cross sect. no, s	Opt. angle of attack	Twist angle (deg)	Blade setting angle (deg)	Chord length (m)	Airfoil max. thickness (m)
1	6	48	42	0.1783	0.0214
2	6	30	24	0.3334	0.0400
3	6	22	16	0.2495	0.0299
4	6	17	11	0.2411	0.0289
5	6	14	8	0.1794	0.0215
6	6	11	5	0.1685	0.0202
7	6	10	4	0.1426	0.0171
8	6	9	3	0.1301	0.0156
9	6	8	2	0.1142	0.0137
10	6	7	1	0.0963	0.0116
11	6	6	0	0.0947	0.0114

2.6 Linearization of Chord Length

Linearization of chord length is needed because smooth geometric construction and aesthetic option will be required for the blade. The chords and the blade angles are calculated vary in a non-linear manner along the blade. These kinds of blades are usually difficult to manufacture and lead to an uneconomic use of materials. To reduce these difficulties, it is required to linearize the chords and the blade angles.

It is required to linearize the values of 'c' between r = 0.5R and r = R without too much deviation to the computed theoretical values. The chord length, c can be linearized with the following way:

$$c = a_1 r + a_2 \quad (12)$$

With the values of chord length at r = 0.8638m and r = 1.7276m, the constants a_1 and a_2 can be calculated by solving the two equations from two different values of radius.

$a_1 = -0.0908$, $a_2 = +0.2516$

$\therefore c = -0.0908\, r + 0.2516$

Table 3. Approximated values of chord length

Cross sect. no, s	Radius (m)	Exact chord length(m)	Linearized chord length (m)	Deviation (m)
1	0.1728	0.1783	0.1783	0
2	0.3283	0.3334	0.2218	0.1116
3	0.4833	0.2495	0.2077	0.0418
4	0.6393	0.2411	0.1936	0.0476
5	0.7948	0.1794	0.1794	0
6	0.9503	0.1685	0.1653	0.0032
7	1.1058	0.1426	0.1512	-0.0086
8	1.2613	0.1301	0.1371	-0.0070
9	1.4168	0.1142	0.1230	-0.0088
10	1.5723	0.0963	0.1088	-0.0125
11	1.7276	0.0947	0.0947	0

2.7 Velocity Components of the Blade

Linear velocity at each element, $\omega_i = r_{ei}\, \Omega$ (13)

Angular velocity, $\Omega = 2\pi N/60$ (14)
$= 28.4233$ rad/s

Rotor Speed, $N = 60\lambda\, v_{rated}/(2\pi R)$ (15)
$= 271.422$ rpm

Radius at center of element (1),
$r_{e1} = 0.1728+dr/2$ and $r_{ei} = r_{ei-1}+dr/2$ (16)

Relative wind velocity at each element,

$$v_i = (v_{rated}^2 + \omega_i^2)^{0.5} \quad (17)$$

Table 4. Velocity components of the blade

Section element number, i	Equivalent radius (m)	Rated wind speed (m/s)	Linear velocity (m/s)	Relative wind speed (m/s)
1	0.2506	8.184	7.1229	10.8496
2	0.4061	8.184	11.5427	14.1496
3	0.5616	8.184	15.9625	17.9382
4	0.7171	8.184	20.3824	21.9641
5	0.8726	8.184	24.8022	26.1176
6	1.0281	8.184	29.2220	30.3464
7	1.1836	8.184	33.6418	34.6229
8	1.3391	8.184	38.0616	38.9315
9	1.4946	8.184	42.4815	43.2626
10	1.6501	8.184	46.9013	47.6100

2.8 Lift and Drag Forces of Each Section

$$dF_{Li} = 0.5\ \rho_{air}\ dA_b\ v_i^2\ C_L \quad (18)$$

$$dF_{Di} = 0.5\ \rho_{air}\ dA_b\ v_i^2\ C_D \quad (19)$$

Elemental area,

$$dA_{bi} = 0.5(c_s \cos \beta_s + c_{s+1} \cos \beta_{s+1})\ dr \quad (20)$$

Table 5. Lift and drag forces on each blade section

Section element number, i	Section area (m^2)	Relative velocity (m/s)	Section Lift force(N)	Section Drag force(N)
1	0.0261	10.8496	1.9368	0.0712
2	0.0313	14.1496	3.9574	0.1451
3	0.0303	17.9382	6.1571	0.2258
4	0.0286	21.9641	8.7130	0.3195
5	0.0266	26.1176	11.4583	0.4202
6	0.0245	30.3464	14.2480	0.5225
7	0.0224	34.6229	16.9570	0.6219
8	0.0202	38.9315	19.3342	0.7091
9	0.0180	43.2626	21.2751	0.7803
10	0.0158	47.6100	22.6166	0.8295

Total lift forces exerted on each blade can be obtained by summation of all lift forces dF_{L1} to dF_{L10}. Total lift force of each blade, F_L is 126.6535N and that for three blade wind generator is 379.9605N.

Total drag forces exerted on each blade can be obtained by summation of all lift forces dF_{D1} to dF_{D10}. Total drag force of each blade, F_D is 4.6451N and that for three blade wind generator is 13.9353N.

Total lift force per total drag force is 27.2679. This value must be equal to maximum C_L/C_D.

2.9 Thrust and Moment Forces on Blade

Thrust force of each element,

$$dF_{Ti} = dF_{Li} \cos \phi_i + dF_{Di} \sin \phi_i \quad (21)$$

Moment force of each element,

$$dF_{Mi} = dF_{Li} \sin \phi_i - dF_{Di} \cos \phi_i \quad (22)$$

Table 6. Thrust and moment forces on each blade section

Section element number, i	Thrust Force (N)	Moment Force (N)
1	1.3489	1.3917
2	3.4998	1.8530
3	5.7933	2.0971
4	8.4257	2.2419
5	11.2196	2.3643
6	14.0859	2.2058
7	16.8074	2.3321
8	19.2071	2.3242
9	21.1767	2.1882
10	23.2713	1.9330

Total thrust force exerted on each blade can be obtained by summation of dF_{T1} to dF_{T10}. Total thrust force of each blade, F_T is 124.8357N and that for three blade wind generator is 374.5071N.

Total moment force exerted on each blade can be obtained by summation of dF_{M1} to dF_{M10}. Total moment force of each blade, F_M is 20.9313N and that for three blade wind generator is 62.7939N.

2.10 Available Power from Designed Blade

Moment of each element, $dM_i = dF_{Mi}\ r_{ei}$ (23)

Power of each element, $dP_i = \Omega\ dM_i$ (24)

Table 7. Moment and power on each blade section

Section element number, i	Moment(N-m)	Power(W)
1	0.3488	9.9141
2	0.7525	21.3885
3	1.1777	33.4741
4	1.6077	45.6961
5	2.0631	58.6401
6	2.2678	64.4584
7	2.7603	78.4568
8	3.1123	88.4618

9	3.2705	92.9584
10	3.1896	90.6589

Total moment of each blade can be obtained by summation of dM_1 to dM_{10}. Total moment of each blade, M is 20.5503N-m and that for three blade wind generator is 61.6509N-m.

Total power generated by each blade can be obtained by summation of dP_1 to dP_{10}.Total power of each blade, P is 584.1072 W and total power extracted by three blade wind generator at design wind speed 8.184 m/s is 1.7523kW.

The generator output power is calculated by multiplying mechanical efficiency (96%), and generator efficiency (70%).

P_e= 1.7523x 0.96 x 0.7 = 1.1776kW

For this design, the effect of wake, induction and tip loss factor are not considered. These effect may cause a slightly decrease of power. However, the designed wind turbine is enough to generate required 1 kW power.

3. STRENGTH CHECK

After calculating the required parameters of the blade, the blade 3D solid model can be created in SolidWorks and so that strength checks on blade can be made by simulating.

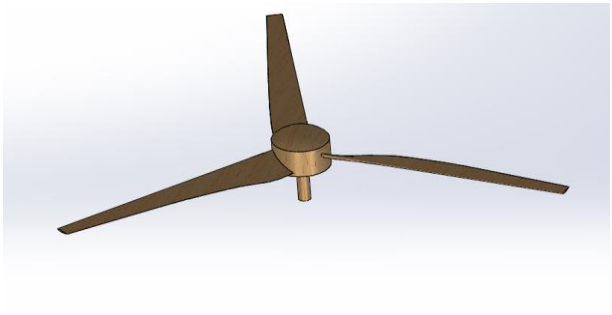

Figure 6. The 3D rotor of wind turbine

Table 8. Complete design parameters of the blade

C-S No.	Radius (m)	λ_r	α (°)	ϕ (°)	β (°)	c (m)	t (m)
1	0.1728	0.60	6	48	42	0.1783	0.0214
2	0.3283	1.14	6	30	24	0.3334	0.0400
3	0.4833	1.68	6	22	16	0.2495	0.0299
4	0.6393	2.22	6	17	11	0.2411	0.0289
5	0.7948	2.76	6	14	8	0.1794	0.0215
6	0.9503	3.30	6	11	5	0.1685	0.0202
7	1.1058	3.84	6	10	4	0.1426	0.0171
8	1.2613	4.38	6	9	3	0.1301	0.0156
9	1.4168	4.92	6	8	2	0.1142	0.0137
10	1.5723	5.46	6	7	1	0.0963	0.0116
11	1.7276	6.00	6	6	0	0.0947	0.0114

It is needed to make some hand calculation in order to examine the stress and deformation on the blade. Moreover, some factors are also necessary for that.

First of all, the solidity (the area ratio of blade and rotor) of the wind turbine must be known. Now, it has to use again the equation of solidity but insert the average value of chord length for (c).

$$\text{Solidity}, \quad \sigma = B\, c_{avg}/(2\pi R) \tag{25}$$

From design, c_{avg} = 0.1753 m, R = 1.7276m, B = 3

Therefore, σ = 0.04844

$$\text{Total Blade Area} = \text{Solidity} \times \text{Rotor Swept Area} \tag{26}$$

Solidity = 0.04844

Rotor swept area = 9.3763m^2

∴ Total blade area = 0.4542m^2

$$\text{Area of each blade, } A_b = \text{Total blade area}/3 \tag{27}$$

$= 0.1514m^2$

Now calculate pressures and forces of lift and drag,

$$F_L = 0.5\, \rho_{air}\, A_b\, v^2\, C_L \tag{28}$$

$$F_D = 0.5\, \rho_{air}\, A_b\, v^2\, C_D \tag{29}$$

F_L = 6.4033N, F_D = 0.2348N

P_L = 42.2939 N/m^2, P_D = 1.5509 N/m^2

It is necessary to consider the centrifugal forces due to the blade mass and centrifugal stresses acting on the blades.

$$F_c = W.SR.\, v^2/(9.81 d_{CG}) \tag{30}$$

Where,

F_c = centrifugal force, W = blade weight

v = rated wind speed, SR= Speed ratio at blade C.G

d_{CG}= distance between the rotor center and blade C.G

Structural analysis finds displacement, strains and stresses. If solid elements are used, then three displacement components (three translations) per node must be calculated. With shell and beam elements, six displacements components (three translations and three rotations) must be calculated.

There are two commonly used failure criteria: Von Mises Stress failure Criterion and Maximum Normal stress Criterion. Von Mises stress, also known as Huber stress, is a measure that accounts for all six stress components of a general 3D state of stress. The Von Mises equivalent stress can be computed as:

$$\sigma_{VM}=[0.5\{(\sigma_x-\sigma_y)^2+(\sigma_y-\sigma_z)^2+(\sigma_z-\sigma_x)^2\}+3(\tau_{xy}^2+\tau_{yz}^2+\tau_{zx}^2)]^{0.5} \tag{31}$$

Numerical simulation procedures include modeling geometry, meshing, adding material properties, applying loads and investigating stress.

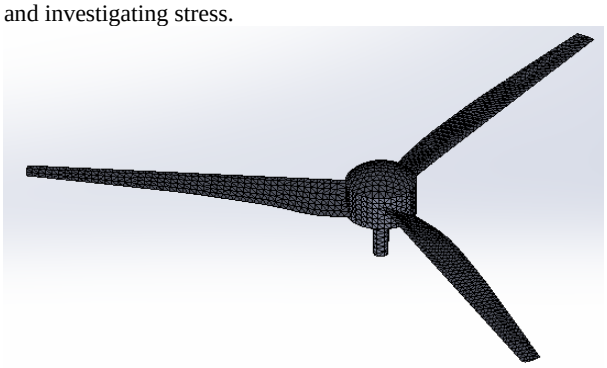

Figure 7. The rotor after meshing

Table 9. The material properties of Balsa Wood

Type	Magnitude	Unit

Elastic Modulus	2999.999232	Mpa
Poisson`s Ratio	0.29	-
Shear Modulus	299.9999105	Mpa
Mass Density	159.99	kg/m^3
Yield Strength	19.999972	Mpa
Thermal Conductivity	0.05	W/(m.K)

After adding material properties of Balsa Wood, simulation has to be made repeatedly from cut-in wind speed 2.8644m/s to cut-out speed 12.276m/s and increment is 2m/s.

Finally, it can be seen that the maximum stress occurs at the blade root. In Figure 8, the maximum stress is shown in red color and the blade is like a cantilever beam because the maximum stress is at the fixed end of the blade.

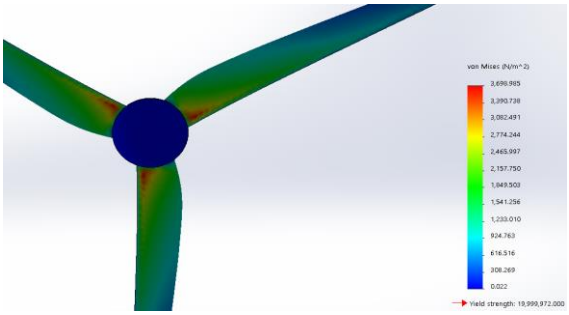

Figure 8. Stress distributions on the blades

After calculating lift and drag forces acting on the blade, it must be found that the lift and drag forces will not cause stress as much as centrifugal force does.

However, the Von Mises stress which is varied with wind speed must be determined because aerodynamic and centrifugal forces are acting on the blade. After making stress simulation, it is necessary to check whether the selected material can bear the maximum stress.

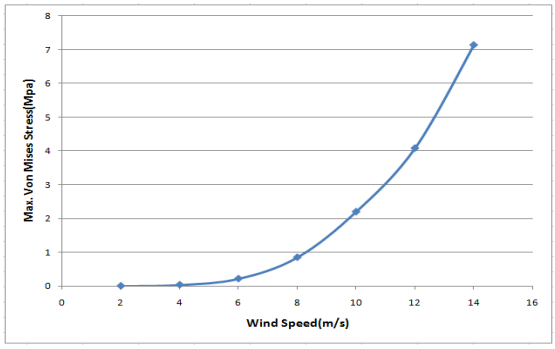

Figure 9. Max. Von Mises Stress at various wind speeds

The selected material, Balsa wood has yield strength of 19.999972 Mpa and then the working stress can be calculated by considering factor of safety of 3 for dead load condition. Then working stress is 6.6667 Mpa and the combined stress acting on each blade is within the range of acceptable working stress.

4. CONCLUSION

In the first part of this research work, it includes the investigations of expected wind speed in the selected site location. After that, aerodynamic theory has to be studied to calculate wind turbine rotor size and available power from wind source. In this paper, the relations of the blade design derived from Blade Element Momentum theory (BEM) are shortly described. Then, blade chord length, blade twist angle and optimum angle of attack have to be determined. In determining the best angle of attack, the maximum lift coefficient from three similar airfoil shapes has to be investigated by using Comsol Multiphysics Software. Modeling Geometry of blade includes getting coordinate points of selected airfoil NACA- 4412 and generating smooth curve for blade chord length variations by making numerical interpolation in SolidWorks. Then the forces acting on the blade in various directions have to be determined. Numerical simulation of strength check has to be made to investigate the stresses on each blade. In this paper, the work of reducing noising effect of rotating rotor blade, designing of tower, yaw and pitch control systems are not considered yet. However, this paper work will contribute to the development of designing blade structure. The designs of wind turbine blade with wood material are extensively used in many small wind turbines. So, the optimum design and strength check of wind turbine blade are very important for practical fields. Technological University (Thanlyin) has initiated the program of utilizing wind power in its existing energy portfolio. Accordingly, wind power resource assessment campaign, wind farm design, optimization, and power grid system integration studies have been initiated. The present effort of understanding the nature of wind power technological developments, existing performance enhancement methodologies, and developing local expertise and facilities is an initiative to contribute towards the national wind energy development program [5].

5. ACKNOWLEDGMENTS

I greatly appreciate to all teachers from the Department of Mechanical Engineering, Technological University (Thanlyin) who work in Renewable Energy Research.

I would like to give great thanks to Renewable Energy Research Department under Department of Research and Innovation for kind permission to study related on-going research projects.

6. REFERENCES

[1] Thiri Shwe Yi Win, “Design and performance analysis of wind turbine”, Ph.d Thesis, MTU, Myanmar, 2007.

[2] David Wood, “Small Wind Turbines, Analysis, Design, and Application”, Department of Mechanical Engineering, University of Calgary, Canada.

[3] Sathyajith Mathew, “Wind Energy, Fundamentals, Resource Analysis and Economics” in India, 2006.

[4] Grant Ingram, “Wind Turbine Blade Analysis using the Blade Element Momentum Method”, Version 1.1 in October 18, 2011.

[5] Perkins, F.W and Cromack, Duane E, “Wind Turbine Blade Stress Analysis and Natural Frequencies”, Wind Energy Center, University of Massachusetts, USA, 1978.

[6] Peter Jamieson, Garrad Hassan, “Innovation in Wind Turbine Design”, UK, 2011.

[7] R. Nolan Clark, “Small Wind – Planning and Building Successful Installations”, USA, 2014.

[8] Muyiwa Adaramola, "Wind Turbine Technology-Principle and Design", Nigeria, 2014.

[9] Willem Nijhoff, "Syllabus for Irrigation with Windmills Technical Aspects", Technical Development with Developing Countries, Netherlands, January, 1982.

[10] Povl Brondsted and P. L. Nijssen, "Advances in Wind Turbine Blade Design and Materials", UK, 2013.

[11] Bharath Koratagere Srinivasa Raju, "Design Optimization of a Wind Turbine Blade", USA, 2011.

International Journal of Science and Engineering Applications
Volume 7–Issue 06,101-102, 2018, ISSN:-2319–7560

Use of Waste Water from Overflowing Village Ponds in Irrigation by using Solar Powered Micro Irrigation Infrastructure

Neeraj Sharma
Executive Engineer
Command Area Development Authority
Kurukshetra, India

Sumit Kumar
Sub Divisional Officer
Command Area Development Authority
Kurukshetra, India

Barjinder Singh
Assistant
Command Area Development Authority
Kurukshetra, India

Abstract: With a view of augmenting water for irrigation purpose & assured supply to the every field, a new intervention has been proposed for utilising surplus water from overflowing ponds in the villages. Working on these lines, Installation of Solar Powered Micro Irrigation Infrastructure has been proposed by selecting the nearby area of the overflowing village ponds by providing common infrastructure with components Sedimentation tank near pond, Pumping Unit (Solar Powered), Filtration units, HDPE pipe network/Hydrant/Outlet assembly, Valves etc with Drip/Sprinkler irrigation sets. The sedimentation chamber will be constructed to settle out the coarse particle thereby providing clear water to the fields. A solar pump of the required capacity will be installed, which will be connected to a filtration unit and after filtration mains and sub mains will be laid by using HDPE pipes. One hydrant will be provided average on 4 acres. It is also proposed to provide one set of sprinklers to the Water User Association for their use to initiate them into use of Micro Irrigation. In this manner, this pilot project will be able to bring new area under irrigation and also gainfully utilise surplus water, otherwise going waste.

Keywords: Solar, Micro Irrigation, Overflowing Village Ponds, Irrigation Efficiency.

1. INTRODUCTION

There are small water bodies either man made or natural, which have been in use since ages. They are traditional water harvesting structures and the water stored in these structures is commonly used for washing/bathing for animals and raising fish. These small water bodies can play an important role in improving the ecological system and help to maintain biological diversity. In the state, the ponds are used for variety of applications. The role of water harvesting systems in semi arid and arid zone is to provide life saving irrigation to low duty crops in the monsoon season and if possible one or two irrigation to raise crop in the dry season. In canal command area a rapid decline of available irrigation water has been observed in many parts of the state due to scarcity of rainfall and increasing demand for water from non agricultural sector. Thus, water for irrigation is becoming both scare and expensive. The problem is more aggravated when ground water is saline and not fit for irrigation use. One characteristic feature of every village is the presence of village pond. Whereas presence of one pond in each village is normal feature, bigger villages also have more than one pond. All the waste water from the village households flows into these ponds. Over the years these ponds have played a major role in day to day activities of village community. With the increase in piped drinking water supply system to the households in villages, the water flowing into these ponds have increased considerably over the years. Often village ponds are seen overflowing, as there is continuous flow of water into these ponds. The stagnant water in these ponds have also lead to various health hazards in the villages besides numerous other environmental, economic and social impacts. Very few ponds have drainage systems wherein the water from village ponds could be drained, so that pond could be cleaned. It is commonly said that cleanliness of a village can be gauged from the status of village pond. The water in ponds is generally household or livestock waste water, which is not at all hazardous for use in irrigating crops. Although there are scattered instances wherein the farmers of villages are utilizing water from ponds for irrigation but these are mostly on temporary basis. This activity coupled with irrigation pipeline shall be immensely beneficial for village community. The utilization of pond water for irrigation will itself help in rejuvenation of ponds as there shall be no stagnant waters in the ponds

2. METHODOLOGY

Solar Powered Micro Irrigation Infrastructure in the Overflowing village pond Commands has been installed by providing Sedimentation tank near Pond, Pumping Unit (Solar Powered), Filtration units, HDPE pipe network/Hydrant /Outlet assembly, Valves etc. in the command area of Village Pond, as shown in layout plan Figure-1. Drip/Sprinkler irrigation sets will be installed by the individual farmers in their farm holdings by availing the benefits of subsidy. It is proposed to construct sedimentation tank of appropriate size near pond. Solar powered pumping system has been installed nearby the sedimentation tank with proper filtration systems to avoid any chocking. Water has been carried to entire area selected nearby the Pond through HDPE pipe line network under pressure. The entire pipe network has been buried under ground at 3 feet deep to avoid land acquisition. Water with the requisite pressure for running of the drip/sprinkler set has been made available to each shareholder at his farm holding through the common infrastructure to be operated & maintained by the Water User's Associations.

Figure 1

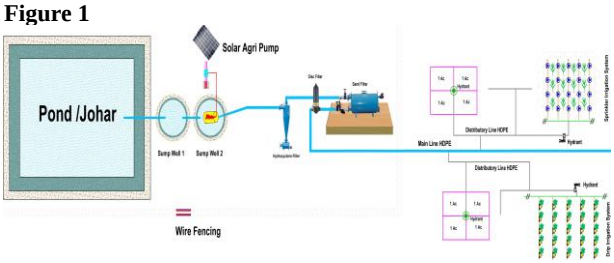

3. DESIGN PARAMETERS

Modified penman method has been used to find out crop water requirement and computed the peak water requirement in rabi & kharif season. In this scheme average water requirement of 2mm/day has been considered. Considering this crop water requirement and capacity of pond along with per capita discharge per day, each component of this scheme shall be designed in such a manner that minimum operating pressure of 2.5Kg/cm^2 available to the farmers on their farm gate. Size of the sedimentation tank has been designed by considering per day inflow in pond and volume of water accumulated as effective outflow in million litres per day. Solar pumping system is a vital part of this scheme and in this scheme solar powered pump has been considered. At least one pump is provided in a block of area 40 to 50 Hactare. Solar pumps of the capacity up to 10 to 20HP is preferred with average working of 6 hours/day. The HP of pump set required is based upon design discharge and total operating head. The total operating head is sum of total static head, friction loses worked out with hazen-williams equation in pipeline network and losses in filtration unit. Pipes in main line and sub-main shall not be below 110 mm (OD) and the size shall be decided based on the criteria to limit the friction loss in the main & sub main keeping the minimum flow velocity in the pipeline as 0.6m/sec.

$$\text{HP of pump set} = \frac{QxH}{75e}.$$

Q = discharge (in LPS)
H = head (in meter)
e = Pumping efficiency

Solar PV array of at least 1100wp capacities has been installed per HP rating of pumping sets and total capacity of the Solar pv array for operation of solar pumping sets has been worked out in such a manner that solar energy generation from the PV power system in no case be lesser than the total energy requirement to run the Micro Irrigation System.

4. CONCLUSION

Significant irrigation from tube wells are being done in various parts of Haryana where water use efficiency is very poor and ground water wastage in shape of flood irrigation is being over exploited. It causes wastage of electricity. Use of micro irrigation infrastructure on overflowing village ponds will reduce the use of tube wells by which ground water will be saved and extra water will be used which was otherwise going waste. More area can be brought under irrigation by using pond waste water, which was otherwise either rain fed or irrigated by tube wells. Where there is no possibility of irrigation through canal commands and ground water is very low, the only solution is creating of Micro Irrigation infrastructure on overflowing village ponds. Where the ground water table is very high with brackish water, there are chances of creating the situation of water logging, which is harmful for soil properties, in these areas, it is essentially required to minimize the flood irrigation by replacing with micro irrigation. Hence, by installation of Solar Powered Micro Irrigation Infrastructure on the over flowing Village pond through integrated approach of supply management and demand management, yield & net sown area will increase. Dependency of tube well & overexploitation of ground water will decrease, and above all it will help to change of the mindset of the farmers towards the use of available water judiciously.

5. REFERENCES

1. Neeraj Sharma, Rajiv Bansal, for Installation of Solar/Grid Powered Micro Irrigation Infrastructure in the Canal Commands in International Journal of Engineering and Technology Volume-56- February 2018.
2. Bucks, D.A. 1993. Micro Irrigation- Worldwide usage report. In Proceedings of Workshop on Micro Irrigation, Sept 2 1993. 15th Congress on Irrigation and Drainage.
3. Neeraj Sharma, Rajiv Bansal, Amit Kumar Raghuvanshi, use of Treated Water from Sewage Treatment Plants in Irrigation by using Solar/Grid Powered Micro Irrigation Infrastructure in International Journal of Science and Engineering Applications Volume 7–Issue 04, 52-53, 2018, ISSN:-2319–7560
4. Batchelor, C., Lovell, C.& Murata, Water User Efficiency of Simple Subsurface Irrigation Systems, In : Proceedings of 7th International Conference on Water and Irrigation, 13-16, May, 1996
5. Howell, T.A. (2001), Enhancing water use efficiency in irrigated agriculture, Agron J 93 (2), 281-289.
6. Hsiao T.C., P. Steduto, and E. Fereres (2007), A Systematic and quantitative approach to improve water use efficiency in agriculture, Irrg. Sci., 25(3), 209-232, doi:10.1007/s00271-007-0063-2.

International Journal of Science and Engineering Applications
Volume 7–Issue 06,103-108, 2018, ISSN:-2319–7560

Analysis of DC Machines Performances

Dr. Tin Win Mon
Department of Electrical Power Engineering
Technological University (Kyaukse)
Kyaukse Town, Mandalay Division, Myanmar

Abstract: This paper presents torque/speed characteristics of electrical machine. Speed is not the same according to various type of electrical machine and field excitation voltage. And then, the speed of separately excited DC machine is inversely proportional to field excitation voltage that show in simulation results. The supply voltage is directly proportional to speed in series motor that show in simulation results. Impedance measurement from variable frequency of the three winding of rotating field machine is presented in this paper. Voltage and current values of Star/Delta conditions of Synchronous machine are simulated by using COM3LAB software, Main Unit, and Electrical Machine Module.

Keywords: Torque/speed; Star/delta; Electrical Machine Module; COM3LAB soft ware

1. INTRODUCTION

Electrical machines are energy converters based on electromagnetic principles. The construction of Electrical machine with moving parts differs from that of machines containing only stationary components. Using the type of energy fed or delivered as a basic three types of electrical machine can be defined:

(i)Motor; (ii) Generator and (iii) Transformer

Electrical machines use electromagnetic forces that appear between energized lines and magnetic fields. This experiment conducts a quantitative study of a rotating coil's dynamic effect in relation to the current. DC machine convert electrical power in the form of DC into mechanical power. They contain stator, rotor, commutator and brushes as the main components.

2. PARAMETERS OF ELECTRICAL MACHINE MODULE

The COM3LAB electrical machine system module is shown in Figure 1. There are included the following parameters;

(1)Stepping motor (200 step in full step operation)

(2) Machine test system (M1: Drive or brake, M2: Testing machine) is required external supply by 12VAC adapter.

(3) Spring balance (+ or – 100Nm, zero point center)

(4) Multichannel oscilloscope

(5)Current/voltage transformer

(6) Three phase generator for induction machines

(7) Asynchronous machine's junction plate

(8) Synchronous Machine's junction plate (the connections of the stator windings Z_1, Z_2 and Z_3)

(9) Synchronous machine: The synchronous machine consists of the following components

-Stator winding Z_1, Z_2, Z_3 and iron cores

-permanently excited rotor

-The reference position is 90 degree after the zero phase passage of the three phase generator

-Stator rotational field indicator

(10) Resistive Load

(11) DC supply for commutator machines (L+,L- :supply for the armature winding; 1L+,1L- : supply for the excitation winding

(12) DC machine's junction plate (A1, A2 : Armature winding,E1,E2 : Shunt winding; D1,D2 :Series winding; F1,F2 : winding for separate excitation)

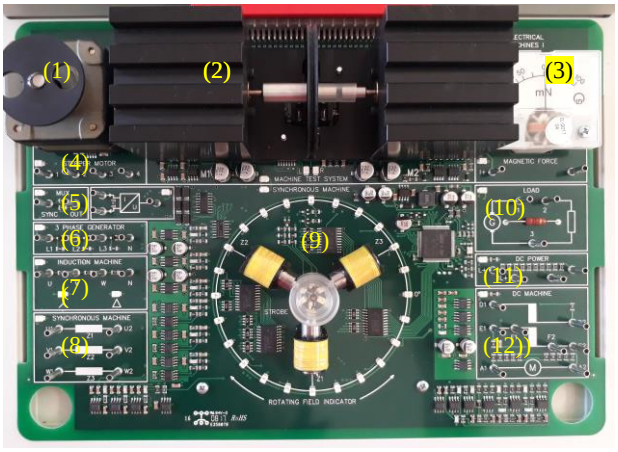

Figure 1. Components of three-phase technology module

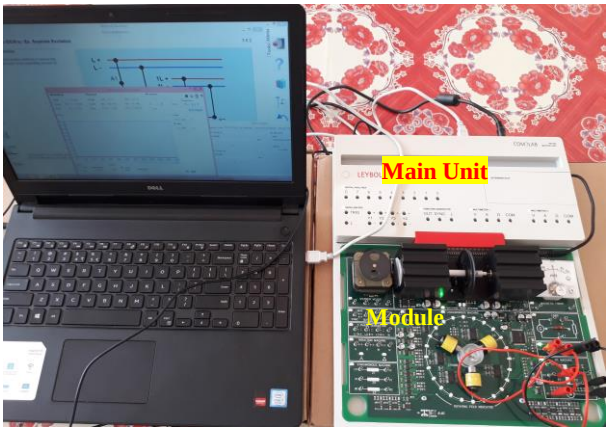

Figure 2.A complete set for simulation

The above Figure 2 is a complete set for simulation. These are Laptop Computer (above P-7), Main Unit, and electrical machine Module.

3. SEPARATELY EXCITED DC MACHINE

.A Separately excited DC machine as in Figure.3, armature and excitation windings have different power supplies (L+ and L- : DC source for armature,1L+ and 1L- : DC source for field winding) . The induced voltage Vi in the DC machine is proportional to the speed n. The torque T generated by the DC machine is proportional to the exciting flux $\emptyset_e$. The torque T is also proportional to the armature current I_A. The maximum torque T_{max} occurs at speed n=0 as the characteristics intersection with the torque's axis .If the excitation and armature voltage have the same polarity, the motor goes clockwise direction. If the excitation and armature voltage have different polarities, the motor goes counterclockwise direction. The torque and speed are proportional to the armature voltage.

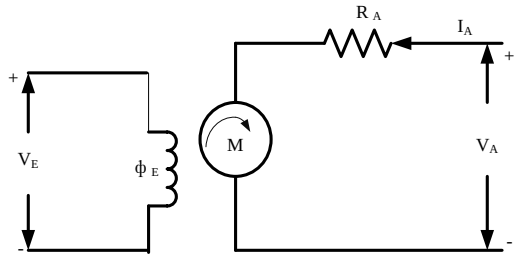

Figure 3. Equivalent circuit of separately excited DC machine

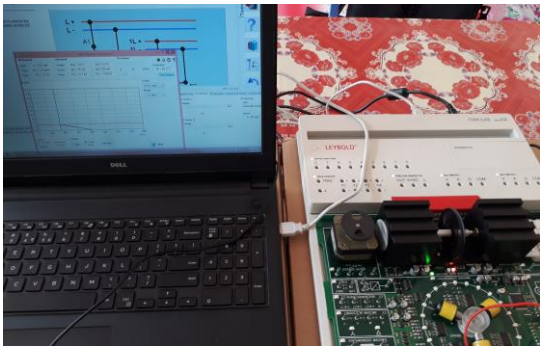

Figure 4. Simulation result of speed measurement

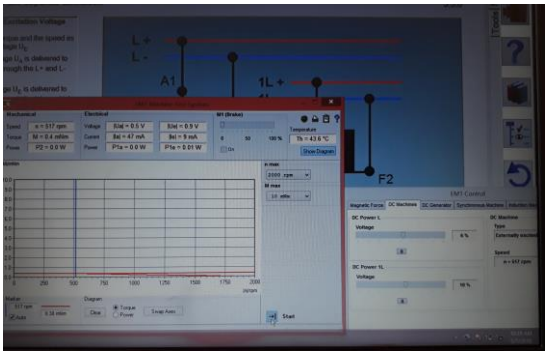

Figure 5. Simulation result of speed measurement

In Figure.4 the excitation voltage is 20% produce the speed is433 rpm. In Figure.5 show the excitation voltage is 10% produce the speed is 517 rpm. So, the speed is inversely proportional to the excitation flux.

4. SHUNT DC MACHINE

In the DC shunt wound operation, the excitation winding E1-E2 and the armature winding A1-A2 are connected in parallel. Due to their high starting torque, series motors used to often be used as railway traction motors. These machines now appear in many housed hold appliances and tools (vacuum cleaners, drills, circular saws, etc) in the form of universal motors. Series motor may not be operated without a load, since its speed would otherwise go unacceptably high. The speed reaches high values at low supply voltage. The torque depends highly on the speed. The torque is greatest at low speeds.

The constant armature voltage is delivered to the shunt motor from DC power through the L+ and L- terminals. The supply voltage 50% are produced the speed 486 rpm as shown inFigure.6.

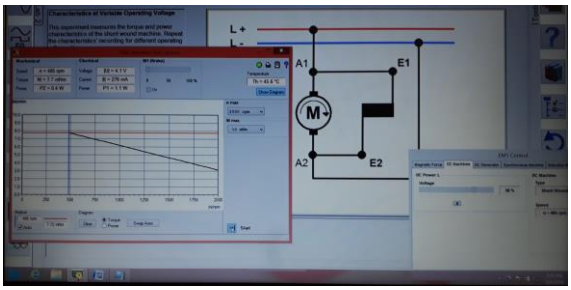

Figure 6. Measuring the speed of shunt DC motor

5. SERIES DC MACHINE

In case of a series motor the flux does not remain constant, or even approximately constant, because the field winding is in series with the load, so that as the load increases so also does the strength of the magnetic field. At first the flux increases approximately in proportion to the load, but as the field approaches saturation, owing to the heavier loads, the increase is not rapid. The effects of temperature changes and of armature reaction may be neglected.

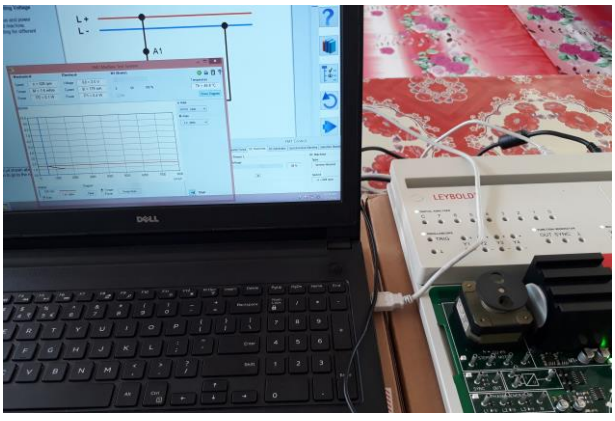

Figure 7. measuring result of speed for series DC motor

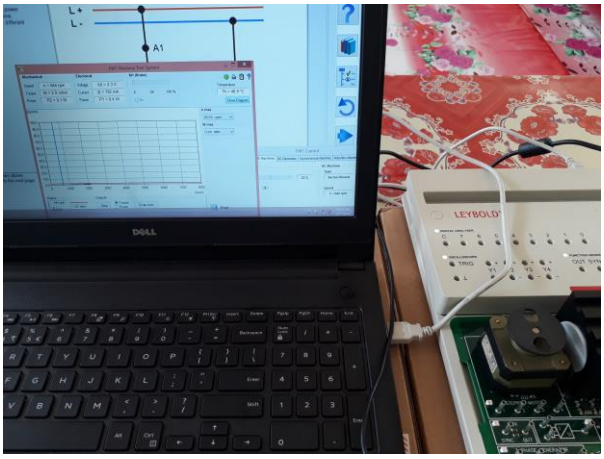

Figure 8. measuring result of speed for series DC motor

As the load torque increases the speed falls rapidly. At low torque the speed becomes very high and machine tends to race. The series motors are used in large starting torque. In Figure.7, DC voltage is 20% produce the speed is 528 rpm. In Figure.8 the DC voltage is 23% produce the speed is 633 rpm. So the speed is directly proportional to the supply DC voltage.

6. ROTATING FIELD MACHINE

Induction and synchronous machines require a revolving magnetic field in the airgap between the stator and the rotor. The rotating field in the airgap essentially determines all rotation field machines' operating behavior. The basic properties of rotating fields and three phase circuit in which the rotating field is a magnetic field whose orientation rotates continuously. The magnetic field's vector tip ideally describes a circular path. Then the magnetic field size's magnitude is constant and in particular independent of the field's direction. The three concentrated coils Z1, Z2 and Z3 generate a very inhomogeneous magnetic rotating field shown in Figure 9.

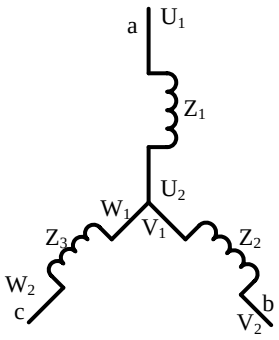

Figure.9 Stator with concentrated winding

The rotational direction changes only when switching two phases. The rotational direction is independent of the stator windings' operation mode. The choice of star or delta connection does not affect the rotational direction. The following Figure.10, measures the line voltages and current s of a star connection by using multimeter 1.The effective line voltages are the same in a balanced star connection. The current's effective values are also equal in all phase conductors.

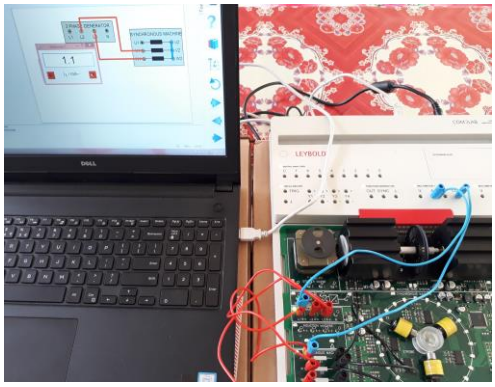

Figure.10 Star connection of rotating field machine

The effective line voltages are the same in a balanced delta connection. The current effective values are also equaled in all phase conductors by using Multimeter 2, measures the delta connection line voltage and line current as shown in Figure 11.

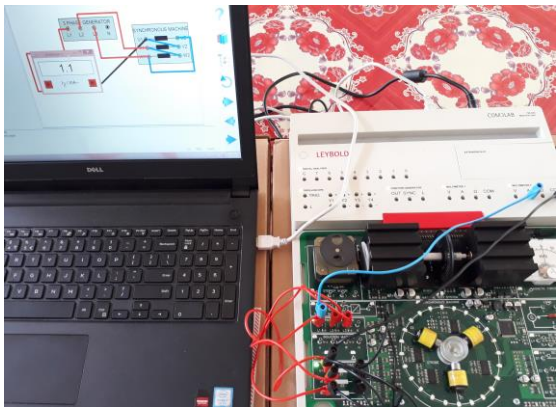

Figure.11 Delta connection of rotating field machine

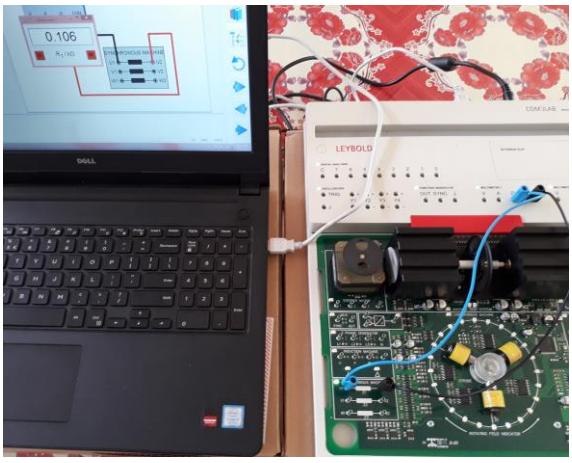

Figure.12 Ohmic resistance measurement of winding U1-U2

The ohmic resistance on the effective resistance of winding Z_1 is 106 ohm as shown in Figure 12. To determine the reactance

of winding Z_1, measure the voltage and current using the multimeter 1 and 2. The impedance measurement result of variable frequency for winding U_1-U_2, V_1-V_2 and W_1-W_2 are as shown in Table 1. The reactance X proportionally increase to the frequency shown in Table 1.

Table.1. Impedance measurement of variable frequency

Winding	f/Hz	Z/Ω	R/Ω	X/Ω
U_1-U_2 (Z_1)	200	852	535	663
	500	1751	541	1665
	1000	3431	513	3392
V_1-V_2 (Z_2)	200	863	524	686
	500	1796	501	1725
	1000	3535	529	3495
W_1-W_2 (Z_3)	200	878	516	71
	500	1843	516	71
	1000	3608	452	3579

6.1 Measuring Power for Star and Delta Connection of Rotating Field Machine

For a measuring power in delta connection and star connection is shown in Figure 13 and 14.

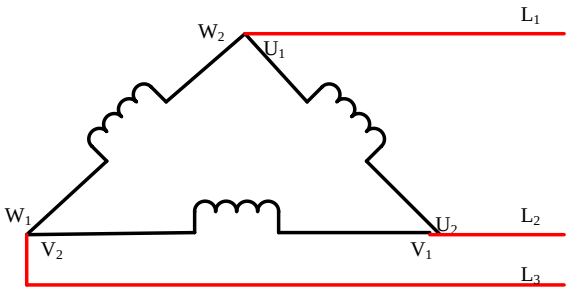

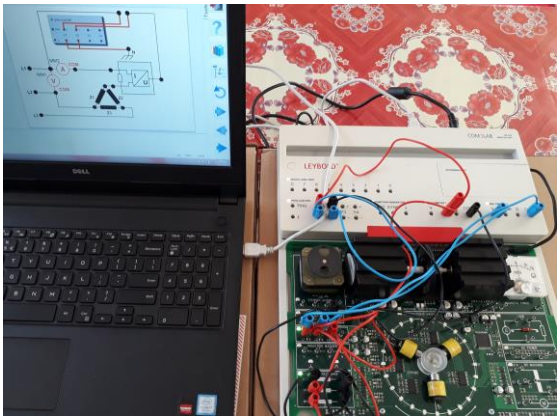

Figure.13 Voltage and current measurement of delta connection

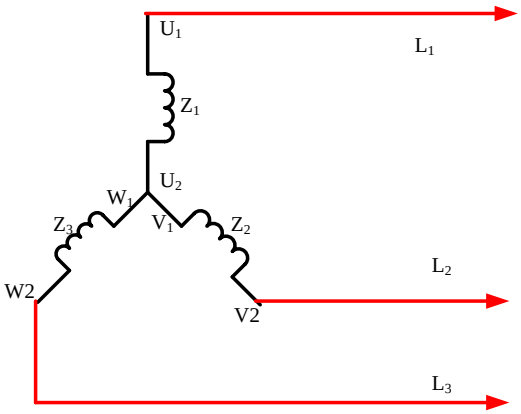

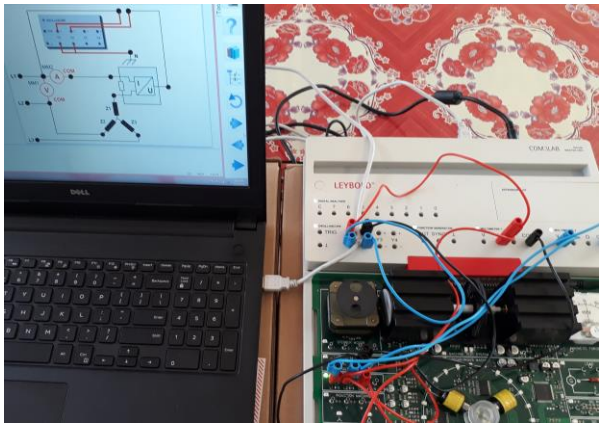

Figure.14 Voltage and current measurement of star connection

$P = \sqrt{3} \times V_L \times I_L \times \cos\phi$ (Watt)

$\Phi = \Delta t/T \times 360$ (degree)

Compare of the measurement results of voltage and current for winding Z_1 (U_1-U_2 terminals) from the above Figure 13 and 14 are presented in the following Table 2.

Table 2. Comparison of voltage and current measurement

Connection	$V_{L1\text{-}L2}$/V	I_1/mA	P/mW
Star (Z_1)	5.2	50	423.17
Delta (Z1)	5.2	150	1271.12

In the three phase load circuit, the supply alternator delivers a constant line to line voltage (in this case $V_{L1\text{-}L2}$ = 5.2V). The line current in delta connection is three times greater than in star connection. The stator in delta connection thus absorbs three times as much active power.

7. SYNCHRONOUS MACHINE

The synchronous machine is an induction machine whose rotor always turns at a perfectly constant speed under a load. The SM's synchronous speed is determined by the stator value's frequency f1 and the machine's number of pore pair p.

The fixed default speed significantly distinguishes the SM's operating behavior from the asynchronous machine's. The synchronous machine consists in a stator with rotating field winding and a rotor whose operation generates a magnetic DC field. In low power machines, permanent magnets generates the rotor's magnetic DC field .The stator resistance R_1 can be neglected for large SM in Figure15.

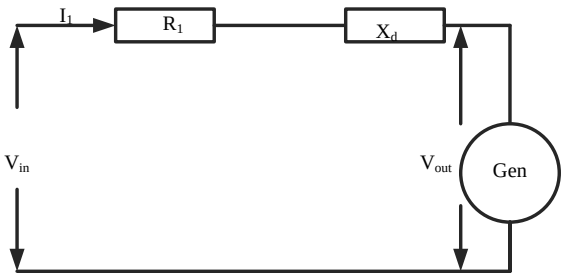

Figure.15. Equavilent circuit of Synchronous machine

In this case , the stator impedance alone is reduced to the synchronous reactance X_d. But this statement does not apply to the COM3LAB software. SM are made for powers above 1GW and are put to use as generators in power stations. Synchronous motors with permanent excitation for small power (1 to 20 kW). SM's can also be used for reactive power compensation.

The three coils of permanently excited synchronous machine Z_1,Z_2 and Z_3 , physically displaced from each other by 120 degree, from an induction machine's stator.An alternator supplies electric energy to the stator coils, which generate a magnetic rotating field at the center of the coils' axles. An enclosed compass needle functions as a rotor in the rotating field shown in Figure 16.

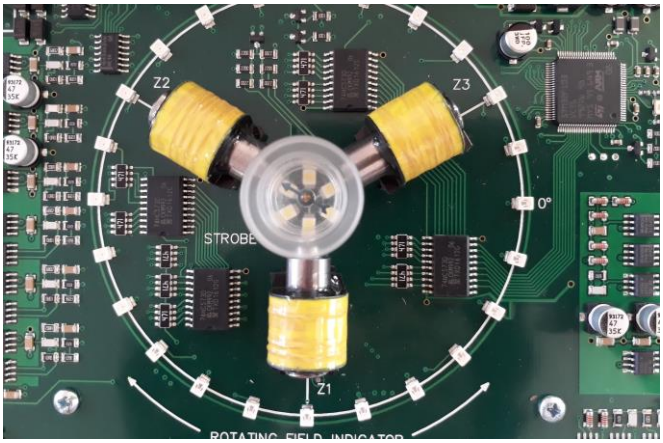

Figure 16. Three coils of synchronous machine with compass needle

In this open setup of the synchronous machine allows for measuring the magnetic field's orientation as a function of current and voltage on the windings. The rotating field show interesting difference between star and delta connections. The synchronous machine has a star connection. Measure the voltage and current of delta and star connection synchronous machine representatively in winding Z_1 as shown in Figure 17 and 18 by using multimeter 1 and 2 .

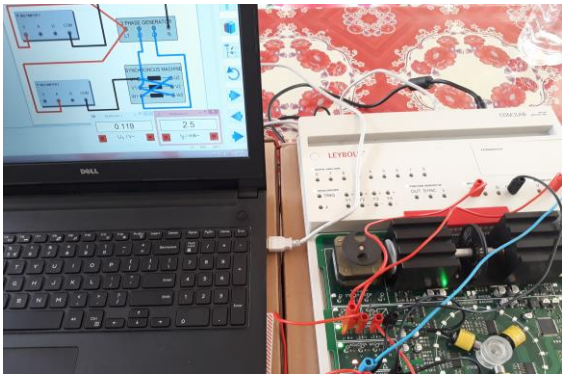

Figure.17.voltage and current measurement of Delta connection

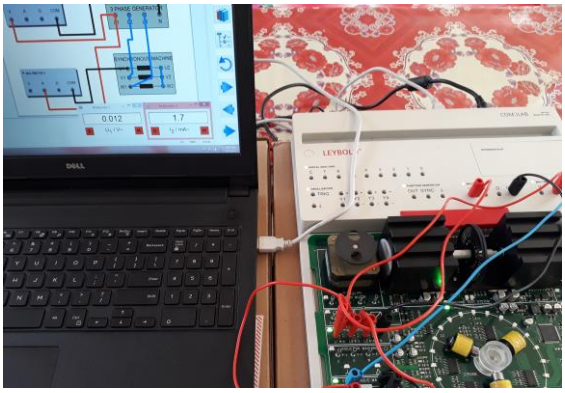

Figure.18.voltage and current measurement of Star connection

The current and voltage can also be measured in the other winding. The concentration factor between star and delta connection is $\sqrt{3}$ for three phase current. The phase in delta connection is delayed by 30degree compared to the star connection. The delta line current is three time greater than in star connection.

8. CONCLUSIONS

In this paper, the first approach with the use of parameters of Electrical Machine Module and Input/Output, Function generator, Multimeter 1 and 2 and Oscilloscope in Master Unit. The second approach with the analysis of electrical machine performance such as separately excited DC machine from various speed simulation results, shunt DC machine and series DC machine performance test. Finally, the comparison of voltage and current measurement for star and delta connection of rotating field machine and synchronous machine. Through this paper analysis of Star symmetrical load, Star asymmetrical load, Delta symmetrical load and delta asymmetrical load was done by simulations.

But in this paper, simulation software of COM3LAB is used to contribute with simulation results. This module is compact and safe for demonstration to technological students because of electrical machine is actually large in range.

9. ACKNOWLEDGMENTS

The author would like to dearly and fully express her deepest thankfulness to her parents and husband for their moral support and kindness, permission to carry out this paper. The author would like to thank for her Rector to Dr. Khin Htike Htike Lwin, Rector of Technological University (Kyaukse), Myanmar. The author would like to express special thanks to all persons whom will concern to support in preparing this paper.

10. REFERENCES

[1]R.K. Agarwal, "Principles of Electrical Machine Design", 2000 Jan, Fourth edition, Dewan Sanjeev kumar kataria Nai Sarak, New Delhi.

[2] P.C.Sen," Principles of Electric Machines and Power Electronics", 1996 Jan, Second edition, John Wiley& Sons, Inc, Canada.

[3] J.B. Gupta, S.Hasan Saeed," Electrical Machines and Automatic Control", 2016, S.K. Kataria&Sons, New Delhi.

[4] J.B. G J.B.Gupta, " Theory and performance of Electrical Machines", 2015 Jan, Fifteenth edition, S.K. Kataria & Sons, New Delhi.

International Journal of Science and Engineering Applications
Volume 7–Issue 06,109-114, 2018, ISSN:-2319–7560

Effect of Road Network on Maintenance of Commercial Vehicles in the Birim Central Municipality

I. L. Mbeah
Department of Heavy Duty and Diesel Mechanics
Kumasi Technical Institute
Kumasi, Ghana

A.K. Arkoh
Department of Mechanical Engineering
Takoradi Technical University
Takoradi, Ghana

E. Acqauh
Department of Mechanical Engineering
Takoradi Technical University
Takoradi, Ghana

Abstract: The study examined the effects and the relationship between the nature of the road network system in the Birim Central Municipality and the routine maintenance schedule by the vehicle manufacturers that are to be observed by vehicle owners and drivers. In addition to that, the study was also meant to find out whether the frequent maintenance as a result of the nature of the road network affects the vehicle owners and drivers income generation. A descriptive survey design was used to analyze the study. The population consisted of vehicle owners, drivers and vehicle mechanics (fitters) totaling hundred (100) randomly selected from the municipality. Questionnaires were designed and used to collect the required data for the study. The data was analyzed using Statistical Package for Social Sciences (SPSS v 16).The study revealed that, the area under-studied had bitumen, gravel and earth roads and most vehicle owners and drivers ply on bitumen because of its accessibility, notwithstanding, they intend to perform more maintenance than those plying on gravel and earth roads which was as a result of poor nature that deters most vehicles. Generally, the nature of gravel and earth roads which are mainly found in rural areas are bad and does not receive regular road maintenance. The results obtained from the analysis indicated clearly that, more than GH¢ 21.00 (61.2%) is spent on weekly maintenance in the area, and this leads to low level of income. Additionally, the results revealed that, the respondents do not refer manufacturer's manuals when performing maintenance on their vehicles as indicated by 96% of them. The road maintenance in the municipality generally is not the best and this makes gravel and earth roads not accessible and motorable and again promotes frequent breakdowns of vehicles.
Based on the findings, recommendations are therefore made for the necessary actions to be taken.

Keywords: Road Network, Schedule Maintenance, Transport, Safety, Profit, Manufacturer's Manual

1. INTRODUCTION

The nature of the road network system in the Birim Central Municipality is a great challenge on the conditions of the vehicles. Transport business has now become a major occupation by the people within the municipality but the nature of road network hinders them from rendering quality services and also prevents them to stick to the maintenance schedule planned for their vehicles within the specified period. Birim Central Municipality is made up of three kinds of roads which comprising bitumen, gravel and earth with which gravel roads form the majority and the bitumen the least. Bitumens are mixture of high-molecular hydrocarbons, methane, naphthene and aromatic series and their oxygen or sulphur derivatives. The major application of bitumen is road construction to ensure rapid movement of goods and services as well as people within the research area. According to [9], asphaltum or tar concrete as artificial material manufactured by compacting a special mixture composed of crushed stone (gravel), sand, mineral powder, bitumen or tar and pitch as a material used in road construction. According to [6], gravel roads can cater heavier traffic and are considered as cheap all-weather roads. The carriageway of this type of road is provided with a camber. These roads are fairly resilient and are suitable to cater for about 100 tonnes of pneumatic tyred vehicles of 60 tonnes of iron tyred traffic per day per lane or average daily traffic between 350-400 vehicles. Earth road is the lowest form of the surface. The nature of these roads in Birim municipality is in a very deplorable state to the extent that, drivers plying on these roads are not able to adhere to the routine maintenance schedule specified by the vehicle manufacturers as a result of constant breakdown of vehicles which needs urgent maintenance response to keep them operating. The bad nature of the roads includes potholes, undulating surfaces and erosion. Adhering to the proper routine vehicle maintenance schedule is important to help keep the vehicle in top running condition and to make profits as far as transport business is concerned [2],[4]. The good nature of road network system is a guarantee to the safe mobility of goods and people from one location to other to enhance business activities. According to [8], high maintenance and operation are important aspect of highway engineering. Involved are the repair and upkeep of surfacing and shoulders, bridges and damaged facilities. Routine vehicle maintenance is the effective way of ensuring that the vehicle is in good condition for day's work. Objectives of maintenance includes; extension of useful life of the vehicles to ensure optimum availability of vehicles for operation to ensure the comfort and safety of personnel's using the vehicles [10].The minimum maintenance to be performed by any vehicle owner or driver is the one stated in the manufacturers maintenance schedule manual. This could be done hourly, weekly, monthly, or yearly, but due to the poor nature of the road network system in the Birim Central Municipality the vehicle owners and drivers perform the maintenance services more often and earlier than stated in the vehicles manual. The routine maintenance to ensure good condition of vehicles covers change of the following; engine oil and filter, tyre and air filter, fuel filter replacement, coolant replacement, transmission service, axle service, battery service, timing belt [3]. No work of this nature has been done to report the effect road network on vehicle maintenance. In view of the above conditions, the present study was undertaken to provide the feedback of the effects that poor nature of the road network has on both commercial vehicles and the rural folks as far as vehicle maintenance is concerned.

2. RESEARCH METHODOLOGY

2.1 Research Design

The study adopted descriptive method to gather the relevant data obtained from the research area. This method was adopted, because the descriptive study seeks to gather information so that a proper presentation and conclusion can be made. This method may be designed to discover whether there is any relationship between two variables [1].

2.2 Study Area

Birim central municipal district is one of the twenty-one-district of the Eastern region of Ghana. The municipal district is located in the southwestern corner of the Eastern Region. The municipal district covers a land size of 1,090 km^2 (420sq mi) and Akim Oda is the capital. The Birim central municipal district is one of the new districts created in 2008 in Ghana. The population settlements of Birim central municipal district is 60,604 per the population and housing census in 2013 [7].

2.3 Population and Sampling Technique

The population in the study refers to the vehicle owners, drivers and mechanics (fitters) and objects that have valuable information to give about the research. The target population for this study was drawn from the Birim Central Municipality consisting of fifty (50) drivers, thirty (30) vehicle owners and twenty (20) vehicle mechanics (fitters). A simple random sampling technique was adopted for data collection in the study.

2.4 Data Collection Instrument

The researcher basically used questionnaires, unstructured interviews, visits and observations to collect the required data study.

2.5 Data Analyses Instrument

The data obtained from the respondents was analysed using the Statistical Package for Social Sciences version (SPSS v 16). This was chosen for easy analysis and a better understanding of the study by interested parties.

3.0 RESULTS AND DISCUSSIONS

Table 1: Types of vehicular roads by occupation χ^2=1.974, p-value=0.373

	Occupation:		
Variables	**Driving**	**Vehicle owner**	**Total**
Bitumen	46	18	64
	76.7%	90.0%	80.0%
Gravel	11	2	13
	18.3%	10.0%	16.2%
Earth	3	0	3
	5.0%	.0%	3.8%
Total	60	20	80
	100.0%	100.0%	100.0%

Presented in Table 1 above shows the type of vehicular roads in the Birim municipality and the results show that more than two-thirds of the respondents (n=64, 80%) reported that they ply on Bitumen roads whereas 13 respondents representing 16.2% reported of Gravel roads while the remaining 3 comprising 3.8% reported of earth. There was no association between the occupation of respondents and the types of vehicular roads in the municipality (χ2=1.974, p-value=0.373).

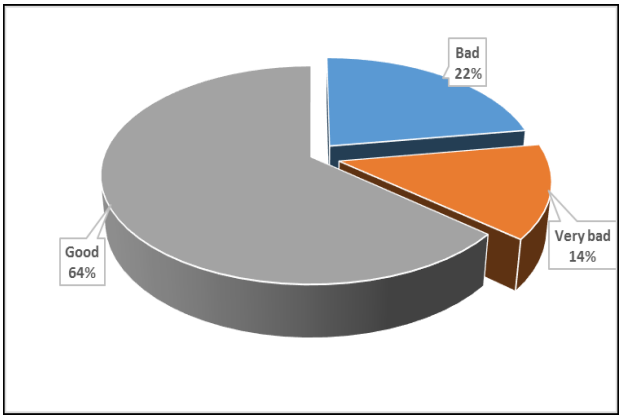

Figure 1: Condition of roads in the Municipality

Table 2: Routine/Periodic maintenance schedule carried out by type of road χ2=6.233, p-value=0.182

	Type of vehicular road			
Variable	**Bitumen**	**Gravel**	**Earth**	**Total**
Daily maintenance	24	2	0	26
	37.5%	15.4%	.0%	32.5%
Weekly maintenance	35	11	3	49
	54.7%	84.6%	100.0%	61.2%
Monthly maintenance	5	0	0	5
	7.8%	.0%	.0%	6.2%
Total	64	13	3	80
	100.0%	100.0%	100.0%	100.0%

Table 2. Is a cross-tabulation of results on the routine/period maintenance schedule carried out by respondents by the type of roads in the municipality? Analysis of the results shows that, more than half of the respondents (n=49, 61.2%) carry out scheduled maintenance weekly, whiles 26 respondents representing 32.5% of the entire respondent population carry out maintenance Daily. The table also shows that majority of the drivers who drive on Bitumen type of road undertake weekly maintenance which represents 35 of the respondents. However, no association was found between responses on the routine/periodic maintenance carried out and they type of road (χ^2 =6.233, p-value=0.182).

Table 3. The nature of the road condition by type of vehicular road χ^2=56.725, p-value<0.001

Condition of Road	Type of vehicular road			
	Bitumen	**Gravel**	**Earth**	**Total**
Bad	11	4	3	18
	17.2%	30.8%	100.0%	22.5%
Very bad	2	9	0	11
	3.1%	69.2%	.0%	13.8%
Good	51	0	0	51
	79.7%	.0%	.0%	63.8%
Total	64	13	3	80
	100.0%	100.0%	100.0%	100.0 %

Table 3 above gives an idea about the condition of vehicular roads in the Birim municipality. The table gives evidence that majority of the roads in the municipality are in good condition as more than half of the respondents (n=51, 63.8%) reported. However, 18 respondents representing 22.5% of the entire population reported that the roads are bad. The results showed a statistically association between the responses of respondents on the condition of roads and the type of vehicular roads in the municipality (χ^2=56.725, p-value<0.001).

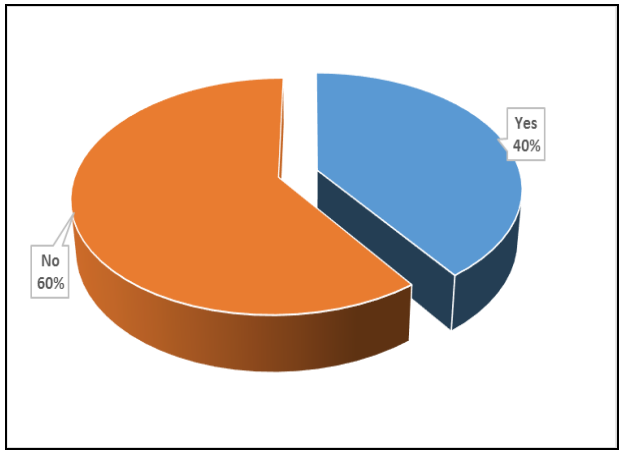

Figure.2. Does the road you ply receive regular road maintenance?

Respondents were asked to indicate whether roads in the municipality receive regular maintenance. Figure.2 shows that 60% of the respondents responded 'No' whereas the remaining 40% responded 'Yes'. Those who answered 'Yes' admitted that the maintenance carried out on the road is only patching of potholes as indicated in the Table 4.

Table 4. Type of road maintenance

Responses	Frequency	Percentage
Patching of potholes	32	100.0
Total	100	100.0

Table 5. Influence of bad nature of road on vehicle maintenance

Responses	**Frequency**	**Percent**
It promotes regular vehicle maintenance	28	100.0
Total	100	100.0

Respondents were asked to indicate the nature of the road in the Birim Municipality. From the responses, all those who responded 'Bad' and 'Very Bad' were asked to indicate whether the 'Bad' nature of the road influences or contributes to vehicle maintenance. The responses being shown in Table 5 shows that all the respondents reported that the 'Bad' nature of the road is a major cause of regular vehicle maintenance.

Table 6. The road condition and cost on maintenance schedule

The nature of the road condition	cost on maintenance schedule			
	Daily maintenance	**Weekly maintenance**	**Monthly maintenance**	**Total**
Bad	1	15	2	18
	3.3%	34.1%	33.3%	22.5%
Very bad	4	7	0	11
	13.3%	15.9%	.0%	13.8%
Good	25	22	4	51
	83.3%	50.0%	66.7%	63.8%
Total	30	44	6	80
	37.5%	55.0%	7.5%	100.0 %

(χ^2=11.934, p-value<.05)Pearson's R = -.303, p<.05

Table 6 shows the relationship between road condition and the cost maintenance carried out. The responses shows that, majority of the respondents (n=44, 55%) reported that, it is expensive to carry out weekly maintenance. Also 30 respondents representing 37.5% of the entire population reported, it is expensive to carry out daily maintenance. However, analysis of the results found a statistically significant association between the nature of roads and cost of maintenance schedule (χ2=11.934, p-value<.05).A statistically significant but week negative Pearson's correlation was found between the variables (Pearson's R = -.303, p<.05) 1 tailed. This suggests that there is a negative linear relationship

between the nature of road and the cost of maintenance schedule where the road gets bad. There is an increase in weekly maintenance schedules which has been found to be expensive. Also the relationship was found to be significant which indicates that the linear relationship is strong.

Table 7. The cost of maintenance every week by routine/periodic maintenance schedule to be carried out

	The cost of maintenance every week			
	GH¢ 5.00-10.00	**GH¢ 11.00-20.00**	**> GH¢ 21.00**	**Total**
Daily maintenance	2	6	18	26
	16.7%	24.0%	41.9%	32.5 %
Weekly maintenance	9	17	23	49
	75.0%	68.0%	53.5%	61.2 %
Monthly maintenance	1	2	2	5
	8.3%	8.0%	4.7%	6.2%
Total	12	25	43	80
	15.0%	31.3%	53.7%	100.0 %

(χ^2=4.002, p-value=.406), Pearson's R = -.207, p=.065

Table 7 is a cross-tabulated results showing the cost of maintenance by the routine/periodic maintenance schedule carried out. Reading horizontally, out of the 80 respondents majority (n=49, 61.2%) carry out weekly maintenance whiles incurring more than GH¢21.00 as the cost of vehicle maintenance every week. Further the 26 respondents representing 32.5% maintain their vehicles daily and out of this, majority (n=18, 41.9%) also incur more than GH¢21.00 as cost of maintenance every week. However, at a (χ^2=4.002, p-value=.406) the results showed no association between the cost of maintenance and the period maintenance schedule carried out by respondents. Again there was a negative correlation between the variables in that a reduction in the routine/periodic maintenance carried out the higher the cost of maintenance and the more maintenance works carried out in the week the slower the cost of maintenance.

Table 8. Cost of maintenance every week by age of vehicle under maintenance.

	Age of vehicle under maintenance			
	1-5 years	**6-10 years**	**11-15 years**	**Total**
GH¢ 5.00-10.00	7	4	1	12
	14.0%	15.4%	25.0%	15.0%
GH¢11.00-20.0	19	5	1	25
	38.0%	19.2%	25.0%	31.2%
> GH¢ 21.00	24	17	2	43
	48.0%	65.4%	50.0%	53.8%
Total	50	26	4	80
	62.5%	32.5%	5.0%	100%

The cost of maintenance per week spent with respect to the age of the vehicle is presented in the Table 8. From the table, it was discovered that more than half of the respondents representing 53.8% spends more than GH¢ 21.00 and 25 out of them also representing 31.2% spends between GH¢ 11.00-20.00 on maintenance every week irrespective of the age of the vehicle whereas 15% of the respondents spend between GH¢ 5.00-10.00.Moreover, vehicles ageing between 6-10 years spend more than GH¢ 21.00 as reported by 65.4% of the respondents as against 48% of vehicles within the ages of 1-5 years as the least.

Table 9. Usage of manufacturer's manual during vehicle maintenance (χ^2=2.778, p-value=0.249)

	Usage of manual for vehicle maintenance		
Variable	**Yes**	**No**	**Total**
Driving	4	56	60
	100.0%	58.3%	60.0%
Vehicle mechanic (fitting)	0	20	20
	.0%	20.8%	20.0%
Vehicle owner	0	20	20
	.0%	20.8%	20.0%
Total	4	96	100
	4.0%	96.0%	100.0%

Table 9 shows the usage of manufacturer's manual during vehicle maintenance. Outcome of the analysis shows that 96% of the respondents do not refer to the manufacturer's manual when carrying out vehicle maintenance. However, 4% of the respondents responded 'Yes'. No association was found between the use of manufacturer's manual during vehicle maintenance and the occupation of respondents (χ2=2.778, p-value=0.24.

3.1 DISCUSSIONS

3.1.1 Types of roads in the municipality and how they influence vehicle maintenance

As more people are into transport business in the Birim Municipality, there must be motorable or accessible roads for plying on them. The municipality is made up of three different kinds of vehicular roads. These include bitumen, gravel and earth. However, individual road type must be able to serve its intended function in the municipality. The initial findings of the study shows that a significant number of respondents 80% ply on bitumen road as against 16.2% who ply on gravel road, only 3.8% of the respondents ply on the earth road. It is a fact that these three types of vehicular roads exist in the municipality to facilitate the free movement of both goods and services and people from different locations to another. From the findings it appears that the majority of both drivers and vehicle owners prefer plying on bitumen road to any type of road. The reason is that bitumen roads are accessible and motorable. The results obtained indicated that, (64%) depicts the condition of the road is good as stated by the majority because they ply on only bitumen road. This response is in

line with [9] that bitumen as a mixture is a durable material for road construction. (25%) of the respondents disagreed to the majority's decision that the road condition generally is good, because they ply on gravel and earth roads which are normally found in the remote areas of the municipality. With regards to the number of days plying on the road in a week and occupation (drivers and vehicle owner), the researcher decided to find out how many days do the respondents use their vehicles on the road because the frequent usage of vehicle on a particular road has a great influence on the rate at which vehicle maintenance is done. Again, the results also indicated that, the respondents perform weekly vehicle maintenance irrespective of the road type as depicted by 61.2% of the analysis from the data received. Daily maintenance is the second to weekly vehicle maintenance and the monthly vehicle maintenance is the least of them as they stand at 32.5% and 6.2% respectively. Vehicles that plied on bitumen type of road undergo more weekly vehicle maintenance, this was because most vehicles plied on bitumen road in the municipality. This study therefore suggests that, those that plied on gravel (84.6%) and earth (100 %) roads carry out weekly vehicle maintenance on their vehicles more than that of bitumen (54 .7%) road type. This is as a result of the poor nature of the road network system in certain part of the municipality.

3.1.2 The effects of the nature of road network in the area on vehicle conditions

The results from the analysis of this section of the study revealed that, the majority of the respondents (79.7%) said that the nature of the road network is fairly good. With regards to both gravel and earth roads it was realized that the nature of the road network system is bad as shown by the analysis of 69.2% and 100% respectively. This indicates that the rural areas of the study area which have most of their roads being gravel and earth are not accessible and motorable and even some of the bitumen road is not in good condition. The respondents who said the nature of road networks are bad, also indicated that, it has a great influence on their vehicle maintenance. The respondents were again made to indicate whether the road they ply receives regular road maintenance and more than half of them (60%) said 'No' to that effect but the rest of the respondents (40%) responded 'Yes'. This portrays that, the road maintenance culture in the municipality is generally poor and its affects the road accessibility. Results shown in (Table 7) indicated that, weekly maintenance (55%) was found to be the expensive maintenance schedule irrespective of the nature of the road condition followed by daily maintenance. In the study area, the results shows that, most vehicles ply on bitumen road (which is fairly good) and as a result have more maintenance schedule (63.8%) as compared to other nature of the road conditions. The results again indicated that, drivers and vehicle owners spends more than GH¢ 21.00 to maintain their vehicles as reported by 53.5% of the respondents with respect to weekly maintenance. With the cost of maintenance every week, the respondents spends more on weekly maintenance schedule (61.2%), next is the daily maintenance schedule as indicated by 32.5% of the respondents. Concerning the age of vehicle and maintenance cost, the researcher realized that the respondents incur more than GH¢ 21.00 representing 53.8% and 31.2% of them spend between GH¢ 11.00-20.00 whereby 15% of the respondents pay between GH¢ 5.00-10.00 to keep their vehicles in good conditions regardless of the age. Meanwhile, the respondents spend more (> GH¢ 21.00) on vehicles falling between the age bracket of 6-10 years as indicated by 65.4% of them but they spend less in maintaining those in 1-5 years.

3.1.3 The usage of vehicle manufacturer's manuals for vehicle maintenance

The researcher sought to enquire whether the respondents perform their vehicle maintenance under the guidance of the manufacturer's manuals and the study clearly showed that, they do not consult the manufacturer's manuals when carrying out the maintenance on their vehicles. The results revealed that, (96%) of the respondents said 'No' and the remaining of the respondents (4%) answered 'Yes'. Without consultation of vehicle maintenance manuals, it makes it difficult for one to know the kind of maintenance to be carried out and when to do so. [2],[3] Reported that, the best source of information about scheduled maintenance is from the vehicle manufacturers. He again describes manuals as books provided by vehicle manufacturers to users in which rules and regulations which will help in the safe and effective use of their equipment (vehicles) are clearly written. Once the respondents do not refer to manuals, to know the required scheduled maintenance to be performed as stated by manufacturers, it is evidence that the proper vehicle maintenance may not be carried out.

4.0 CONCLUSION

The study has shown that the three kinds of vehicular roads (bitumen, gravel and earth) in the municipality, bitumen is more motorable than the rest but the nature of these roads system is bad and discourages free movement vehicles especially gravel and earth as the majority of road network linking the various rural areas. Owing to this, drivers who ply on these roads (gravel and earth) incur high maintenance cost as a result of frequent breakdown. From the research, it was also found that drivers and vehicle owners perform weekly maintenance more than any other maintenance and also discovered from the poor nature of the road network. The bad nature of the road can be checked by ensuring regular and proper road maintenance such as patching of potholes, grass cutting along the roads, reshaping etc. to make it more accessible but the study indicated that the roads do not receive regular and proper maintenance as they should and the only maintenance carried out is patching of potholes which is not even as regular to keep the road halfway maintained in shape for easy accessibility. Drivers and vehicle owners pay more to maintain their vehicles as the study indicated and it found to be the reason for income reduction as far as transport business in the area is concerned and if they continue to spend more on maintenance can discourage them from performing the regular routine maintenance of their vehicles. Furthermore, they pay more once again to maintain their vehicles as they are getting older within the age range of 6-10 years. Drivers, vehicle owners as well as vehicle mechanics do not refer the manufacturers' manuals which contain the key instructions for maintaining the vehicles.

5.0 ACKNOWLEDGMENTS

The authors wish to express sincere gratitude to
Head of the commercial drivers' union at the Birim central municipal, in the Eastern Region of Ghana for organizing the drivers for the collection of data.

6.0 REFERENCES

[1.] Agyedu et al (2011). Teach Yourself Research Methods. Kumasi, pp. 91, 92

[2.] Ahmed Zeza (2015). Scheduling Preventive Maintenance for a Non-periodically Inspected Deteriorating System. International Journal or Reliability, Quality and Safety Engineering Vol.22 No. 6(2015) 1556029

[3.] Ashok Leyland, Operator Manual (2011). Ashok Leyland, Engineering Your Tomorrows. India, Falcon Euro-III, pp.5.3-5.27

[4.] Baido F et al (2017). Assessing Maintenance Management Practices on Public Mass Transit Buses in Ghana, International Journal of Engineering and Management Invention, Vol. 02//issue02//April 2017

[5.] Deere (2000). Shop Manual JD-201 (I&T Shop Service), I & T Shop Manuals Volume 201 of I & T Shop Service

[6.] Bindra S. P. (2001). A Course in Highway Engineering. New Delhi, Dhanpat Rai Publication (P) Ltd, pp. 21, 55, 579, 580

[7.] https://en.m.wikipedia.org/wiki/Birim_Central_Municipal_District assessed on 06/06/2018

[8.] Paker (1984). High way Construction and Maintenance: Proceedings of Seminar K Held at PTRC Transport and Planning Summer Annual Meeting, University of Sussex, England.

[9.] Komar A. (1987). Building Materials and Components. Moscow, Mir Publishers, pp.419, 425

[10.] Thillainayagam R, (1996). Fleet Maintenance Management-A Book of Readings. London, Central Institute of Transport Pune – 411026, pp 44, 45